Design of Non-orthogonal Multiple Access Enhanced Backscatter Communication

Jing Guo, *Member, IEEE*, Xiangyun Zhou, *Senior Member, IEEE*,
Salman Durrani, *Senior Member, IEEE*, and Halim Yanikomeroglu, *Fellow, IEEE*

***Abstract*— Backscatter communication (BackCom), which allows a backscatter node (BN) to communicate with the reader by modulating and reflecting the incident continuous wave from the reader, is considered as a promising solution to power the future Internet-of-Things. In this paper, we consider a single BackCom system, where multiple BNs are served by a reader. We propose to use the power-domain non-orthogonal multiple access (NOMA), i.e., multiplexing the BNs in different regions or with different backscattered power levels, to enhance the spectrum efficiency of the BackCom system. To better exploit power-domain NOMA, we propose to set the reflection coefficients for multiplexed BNs to be different. Based on this considered model, we develop the reflection coefficient selection criteria. To illustrate the enhanced system with the proposed criteria, we analyze the performance of BackCom system in terms of the average number of bits that can be successfully decoded by the reader for two-node pairing case and the average number of successful BNs for the general multiplexing case. Our results show that NOMA achieves the much better performance gain in the BackCom system as compared to its performance gain in the conventional system, which highlights the importance of applying NOMA to the BackCom system.**

***Index Terms*—Backscatter communication, reflection coefficient design, non-orthogonal multiple access, user pairing, interference networks.**

I. Introduction

To provide ubiquitous connectivity among tens of billions devices, the internet-of-things (IoT) is envisaged as one of the key technology trends for the fifth generation (5G) system [1]. Under the IoT paradigm, the low-cost devices can automatically communicate with each other without human intervention. Nonetheless, with the development of IoT technology, there are currently many research challenges needed to be addressed, one of them being the energy issue [2], [3]. For those devices where the battery replacement can be very costly, the energy harvesting becomes a desirable approach to maintain the functionality of devices for a long period. It is worthy to note that the energy harvesting can be very compatible with most IoT devices, because these devices only consume a small amount of energy [2], [4].

One of the promising energy harvesting techniques is the backscatter communication (BackCom) [5]. A BackCom system generally has two main components, a reader and a backscatter node (BN). The BN does not have any active radio frequency (RF) component, and it reflects and modulates the incident single-tone sinusoidal continuous wave (CW) from the reader for the uplink communication. The reflection is achieved by intentionally mismatching the antennas input impedance and the signal encoding is achieved by varying the antenna impedance [6]. The BN can also harvest the energy from the CW signal. These energy-saving features make the BackCom system become a prospective candidate for IoT. Note that the BackCom system is different from the wireless powered network (WPN) with harvest-then-transmit protocol (i.e., the nodes use the harvested energy to support the information transmission). The nodes in WPNs contain active RF components which consume additional energy. Hence, the nodes in WPNs may not support frequent data transmission. However, for the BNs in BackCom systems, the power for information transmission comes from the reader and this characteristic potentially allows for more frequent data transmission.

The backscatter technique is commonly used in the radio frequency identification systems (RFID) which usually accommodate the short range communication (i.e., several meters) [6], [7]. Recently, the BackCom system has been proposed for providing longer range communications, e.g., by installation of battery units and supporting low-bit rate communications [7], [8], or exploiting the bistatic architectures [9]. Such extended-range BackCom systems have been considered for point-to-point communication [10]–[15] and one-to-many communication [7], [8], [16]–[18]. For the *point-to-point communication*, the physical layer security mechanism was developed in [10], where the reader interferes with the eavesdropper by injecting a randomly generated noise signal which is added to the CW sent to the tag. In [11], for a BackCom system consisting of multiple reader-tag pairs, a multiple access scheme, named as time-hopping full-duplex BackCom, was proposed to avoid interference and enable full-duplex communication. Other works have considered BackCom systems with BNs powered by the ambient RF signal [12], [13] or power beacons [14], [15]. For the *one-to-many communication*, a set of signal and data extraction techniques for the backscatter sensors' information were proposed in [7], where the sensors operate in different subcarrier frequencies. In [8], the authors used the beamforming and frequency-shift keying modulation to minimize the collision in a backscatter sensor network and studied the sensor collision (interference) performance. In [16], an energy beamforming scheme was proposed based

J. Guo, X. Zhou and S. Durrani are with the Research School of Engineering, The Australian National University, Canberra, ACT 2601, Australia (Emails: {jing.guo, xiangyun.zhou, salman.durrani}@anu.edu.au). H. Yanikomeroglu is with the Department of Systems and Computer Engineering, Carleton University, Ottawa, ON K1S 5B6, Canada (E-mail: halim@sce.carleton.ca).

This work was supported by the Australian Research Council's Discovery Project Funding Scheme (Project number DP170100939).

on the backscatter-channel state information and the optimal resource allocation schemes were also obtained to maximize the total utility of harvested energy. In [17], the decoding probability for a certain sensor was derived using stochastic geometry, where three collision resolution techniques (i.e., directional antennas, ultra-narrow band transmissions and successive interference cancellation (SIC)) were incorporated. For an ALOHA-type random access, by applying the machine learning to implement intelligent sensing, the work in [18] presented a framework of backscatter sensing with random encoding at the BNs and the statistic inference at the reader.

In this work, we focus on the uplink communication in a one-to-many BackCom system. To handle the multiple access, non-orthogonal multiple access (NOMA) is employed. By allowing multiple users to be served in the same resource block, NOMA can greatly improve the spectrum efficiency and it is also envisaged as an essential technology for 5G systems [19]. In general, the NOMA technique can be divided into power-domain NOMA and code-domain NOMA. The code-domain NOMA utilizes user-specific spreading sequences for concurrently using the same resource, while the power-domain NOMA exploits the difference in the channel gain among users for multiplexing. The power-domain NOMA has the advantages of low latency and high spectral efficiency [20] and it will be considered in our work. The implementation of uplink power-domain NOMA for cellular communication systems has been investigated in the literature, e.g., [21]–[23]. Also other works have studied the NOMA-enhanced WPNs, e.g., [24]–[26]. Very recently, the authors in [27] investigated NOMA in the context of a power station-powered BackCom system. To implement NOMA, the time spent on energy harvesting for each BN is different, where the optimal time allocation policy was obtained.

Paper contributions: In this paper, we consider a single BackCom system, where one reader serves multiple randomly deployed BNs. We adopt a hybrid power-domain NOMA and time division multiple access (TDMA) to enhance the BackCom system performance. Specifically, we multiplex the BNs in different spatial regions (namely the region division approach) or with different backscattered power levels (namely the power division approach) to implement NOMA. Different from the conventional wireless devices that can actively adjust the transmit power, we set the reflection coefficients for the multiplexed BNs to be different in order to better exploit power-domain NOMA. We make the following major contributions in this paper:

- We propose a NOMA-enhanced BackCom system, where the reflection coefficients for the multiplexed BNs from different groups are set to different values to utilize the power-domain NOMA. Based on the considered system model, we develop criteria for choosing the reflection coefficients for the different groups. To the best of our knowledge, such guidelines have not yet been proposed in the literature.
- We adopt a metric, named as the average number of successfully decoded bits (i.e., the average number of bits can be successfully decoded by the reader in one time slot), to evaluate the system performance. For the most practical case of two-node pairing, we derive the exact analytical closed-form results for the fading-free scenario and semi closed-form results for the fading scenario (cf. Table I). For analytical tractability, under the fading-free and general multiple-node multiplexing case, we analyze a metric, the average number of successful BNs given N multiplexing BNs, which has similar performance trend as the average number of successfully decoded bits. The derived expressions allow us to verify the proposed selection criteria and investigate the impact of system parameters.
- Our numerical results show that, NOMA generally can achieve the much better performance gain in the BackCom system compared to its performance gain in the conventional system. This highlights the importance of incorporating NOMA with the BackCom system.

The remainder of the paper is organized as follows. Section II presents the detailed system model, including the developed NOMA scheme. The proposed reflection coefficient selection criterion is presented in Section III. The definition and the analysis of the considered performance metrics for the fading-free and fading scenarios are given in Sections IV and V, respectively. Section VI presents the numerical and simulation results to study the NOMA-enhanced BackCom system. Finally, conclusions are presented in Section VII.

II. System Model

A. Spatial Model

We consider a BackCom system consisting of a single reader and M BNs (sensors), as illustrated in Fig. 1(a). The coverage zone $\mathcal{S}$ for the reader is assumed to be an annular region specified by the inner and outer radii R_1 and R, where the reader is located at the origin [8], [17]. The M BNs are randomly independently and uniformly distributed inside $\mathcal{S}$, i.e., the location of BNs is modelled as the binomial point process. Consequently, the distribution of the random distance between a BN and the reader, r, is $f_r(r) = \frac{2r}{R^2-R_1^2}$ [28].

B. Channel Model

In this work, we first consider the fading-free channel model, i.e., we use the path-loss to model the wireless communication channel. Thus, for a receiver, its received power from a transmitter is given by $p_t r^{-\alpha}$, where p_t is the transmitter's power, α is the path-loss exponent, and r is the distance between the transmitter and receiver pair, respectively. This fading-free channel model is a reasonable assumption for the BackCom system with strong line-of-sight (LOS) links [17]. This can be justified as follows. The coverage zone for a reader is generally relatively small, especially compared to the cell's coverage region, and the BNs are close to the reader; hence, the communication link is very likely to experience strong LOS fading. In Section V, we will extend the system model to include the fading. Under the fading case, we assume that the fading on the communication link is identically and independently distributed (i.i.d.) Nakagami-m fading. Also we will show that the design intuition gained from the fading-free

This article has been accepted for publication in a future issue of this journal, but has not been fully edited. Content may change prior to final publication. Citation information: DOI 10.1109/TWC.2018.2864741, IEEE Transactions on Wireless Communications

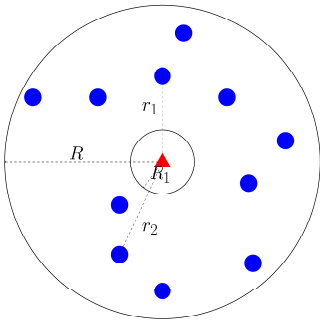

(a) Spatial model (▲ = reader, ● = BNs).

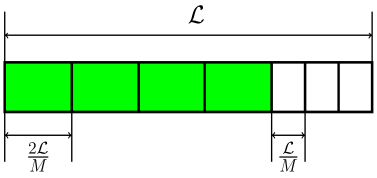

(b) Time slot structure (■ = mini-slot on NOMA, □ = mini-slot on single access).

Fig. 1. Illustration of the system model for two-node pairing case.

scenario can provide a good guideline for LOS fading scenario. The additive white Gaussian noise (AWGN) with noise power $\mathcal{N}$ is also included in the system.

C. Backscatter Communication Model

In general, the BNs do not actively transmit any radio signal. Instead, the communication from a BN to the reader is achieved by reflecting the incident CW signal from the reader. In this work, the reader is assumed to transmit a CW signal for most of the time, while each BN has two states, namely the backscattering state and the waiting state. Fig. 2 depicts the structure of the considered BN; it is mainly composed of the transmitter, receiver, energy harvester, information decoder, micro-controller and variable impedance.

In the *backscattering state*, the BN's transmitter is active and is backscattering the modulated signal via a variable impedance. We consider the binary phase shift keying modulation in this work. To modulate the signal, the in-built micro-controller switches impedances between the two impedance states. These two impedance are assumed to generate two reflection coefficients with the same magnitude (denoted as ξ) but with different phase shift (i.e., zero degree and 180 degree). Combining with our channel model, given that the transmit power of the reader is P_T, the backscattered power at a BN is $\xi P_T r^{-\alpha}$.

In the *waiting state*, the BN stops backscattering and only harvests the energy from the CW signal. The harvested energy is used to power the circuit and sensing functions. We assume that each BN has a relatively large energy storage. The storage battery allows the accumulation of energy with random arrivals and the stored energy can be used to maintain the normal operation of BNs in the long run.

D. Proposed NOMA Scheme

In this section, we describe the proposed NOMA scheme for the BackCom system, which is a contribution of this work. We focus on the uplink communication and employ a hybrid of power-domain NOMA and TDMA. Each time slot lasts $\mathcal{L}$ seconds and $\mathcal{L}$ is further divided into multiple mini-slots depending on the multiplexing situation, which will be explained later in Section II-D2. We assume that all BNs are the same type, e.g., the fixed data rate for each BN is the same, denoted as $\mathcal{R}$ bits/secs, and they all have the same quality of service requirement.

1) Region division for multiplexing: It is widely known that the fundamental principle of implementing power-domain NOMA is to multiplex (group) users with the relatively large channel gain difference on the same spectrum resource [20]. Hence, we utilize the BNs residing in separate regions to implement power-domain NOMA, which is named as the region division approach. Specifically, the reader "virtually" divides the coverage zone into N subregions[2] and the i-th subregion is an annular region specified by the radii R_i and R_{i+1}, where $i \in [1, N]$, $R_i < R_{i+1}$ and $R_{N+1} = R$. The reader randomly picks one BN from each subregion to implement NOMA. Since the BNs are randomly deployed in $\mathcal{S}$, it is possible that the number of BNs in each subregion is not equal. For this unequal number of BNs scenario, the reader will first multiplex N BNs. If the reader cannot further multiplex N BNs, it will then multiplex $N-1$ BNs, $N-2$ BNs and so on and so forth.

2) Time slot structure: Each time slot $\mathcal{L}$ is divided into multiple mini-slots. For the mini-slot used to multiplex n BNs, the time allocated to this mini-slot is assumed to be $n\frac{\mathcal{L}}{M}$. Let us consider $N = 2$ as an example and assume that there are t BNs residing in the first subregion (namely the near subregion) and $M - t$ BNs in the second subregion (namely the far subregion), where $t \leq M/2$ is considered. In the first t mini-slots, where each mini-slot lasts $\frac{2\mathcal{L}}{M}$ seconds, the reader will randomly select one BN from the near subregion and another BN from the far subregion to implement NOMA for each mini-slot. As for the remaining $M - 2t$ BNs in the far subregion, since there are no available BNs in the near subregion to pair them, they can only communicate with the reader in a TDMA fashion in the following $M - 2t$ mini-slots, i.e., each BN is allocated $\frac{\mathcal{L}}{M}$ seconds to backscatter the signal alone. Note that the BNs which are not selected by the reader to backscatter signal on a certain mini-slot are in waiting state. The time slot structure for two-node pairing case is illustrated in Fig. 1(b).

3) Reflection coefficient differentiation and its implementation: To make the difference of channel gains for multiplexing nodes more significant, we consider that the reflection coefficient for the BN belonging to different subregion is different. Let ξ_i denote the reflection coefficient for the BN in the i-th subregion and we set $1 \geq \xi_1 \geq ...\xi_{i-1} \geq \xi_i ... \geq \xi_N > 0$. The reflection coefficient ξ is of importance for the BackCom system with NOMA. In Section III, we will provide design

[2]In this work, we mainly focus on the $N = 2$ case (i.e., NOMA with two-node pairing case), which is widely considered in the literature. The analysis for the general N case will be presented in Section IV-C.

This article has been accepted for publication in a future issue of this journal, but has not been fully edited. Content may change prior to final publication. Citation information: DOI 10.1109/TWC.2018.2864741, IEEE Transactions on Wireless Communications

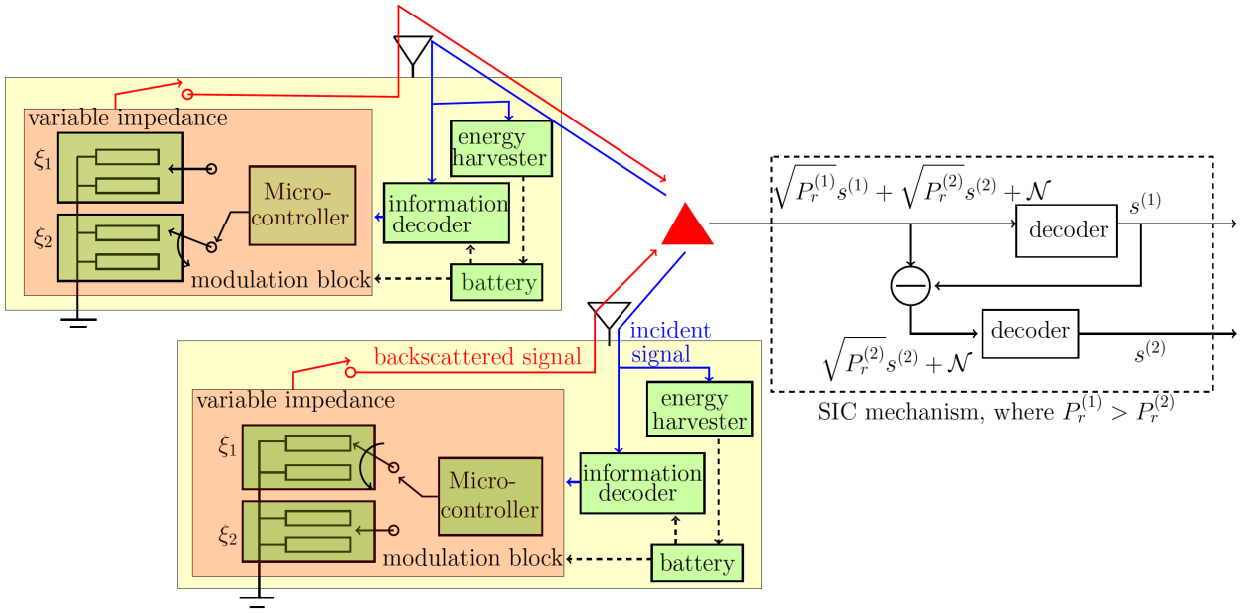

Fig. 2. Illustration of the BackCom with NOMA for $N = 2$ scenario. $P_r^{(1)}$ and $P_r^{(2)}$ denote the stronger signal power and the weaker signal power at the reader, respectively. $s^{(\cdot)}$ denotes the corresponding normalized information signal.

guidelines on how to choose the reflection coefficient for each subregion to improve the system performance.

In order to know which BNs belong to which subregions, the following training procedure is adopted in this work. We assume that each BN has a unique ID, which is known by the reader [8]. Each training phase is divided into M sub-frames and the reader broadcasts the training signal along with a unique ID on each sub-frame. After hearing the unique ID, each BN backscatters this signal in its corresponding sub-frame [16]. Only one BN reflects the signal on one sub-frame. By receiving the backscattered signal, the reader is able to obtain the instantaneous channel state information (CSI) and categorize the BNs into different subregions based on the different power levels. We assume that the obtained instantaneous CSI is perfect. At the same time, each BN can decide which subregion it belongs to according to the received training signal power from the reader, and then switches its impedance pair to the corresponding subregion's impedance pair for the NOMA implementation. Note that, we assume that each BN has N impedance pairs corresponding to the N reflection coefficients for each subregion, from which the micro-controller can select[3]. Additionally, during the training period, all BNs switch to the first impedance pair (e.g., the reflection coefficient is ξ_1).

4) SIC mechanism: NOMA is carried out via the SIC technique at the reader. We assume that the decoding order is always from the strongest signal to the weakest signal[4] and error propagation is also included. For example, the reader firstly detects and decodes the strongest signal, and treats the weaker signal as the interference. If the signal-to-interference-plus-noise ratio (SINR) at the reader is greater than a threshold γ, the strongest signal can be successfully decoded and extracted from the received signal. The reader then decodes the second strongest signal and so on and so forth. If the SINR is below the threshold, the strongest signal cannot be decoded and the reader will not continue to decode the weaker signals. This implies that the remaining weaker signals fail to be decoded as well [29], i.e., all the transmitted data bits are not successfully decoded at all in this case. Fig. 2 illustrates the basic structure for the SIC technique.

[3]Note that N is a pre-defined system parameter. Once N is chosen, the hardware (e.g., the impedance pairs) is fixed.

[4]Under the fading-free scenario, the decoding order is from the nearest BN to the farthest BN. Under the fading case, the signal here implies the instantaneous backscattered signal received at the reader and the strongest signal may not come from the nearest BN.

III. Design Guideline for the Reflection Coefficients

For the conventional communication system implementing power-domain NOMA, the multiplexed devices transmit with different powers in order to gain the benefits from NOMA. Unfortunately, actively updating the transmit power is impossible for BNs, since they are passive devices. Instead, the reflection coefficient is an adjustable system parameter for BNs to enhance the system performance. It is intuitive to set the reflection coefficients for the near subregions as large as possible and set the reflection coefficients for the far subregions as small as possible. Then the question is how small (or large) should the reflection coefficients be for the near (or far) subregions. In this section, we provide a simple design guideline for choosing the reflection coefficients for the subregions, which is presented in the following proposition.

Proposition 1: Based on our system model considered in Section II, to achieve the best system performance, the

reflection coefficient for each subregion should satisfy the following conditions

$$\xi_N \geq \gamma \frac{\mathcal{N} R^{2\alpha}}{P_T}, \tag{1}$$

$$\xi_i \geq \max\left\{\xi_{i+1}, \gamma\left(\sum_{j=i+1}^{N} \xi_j \frac{R_{i+1}^{2\alpha}}{R_j^{2\alpha}} + \frac{\mathcal{N} R_{i+1}^{2\alpha}}{P_T}\right)\right\}, \quad i \leq N-1. \tag{2}$$

For the simplest case where $N = 2$, we have $\xi_2 \geq \gamma \frac{\mathcal{N} R^{2\alpha}}{P_T}$ and $\xi_1 \geq \max\left\{\xi_2, \gamma\left(\xi_2 + \frac{\mathcal{N} R_2^{2\alpha}}{P_T}\right)\right\}$.

Proof: We consider the case of N multiplexing nodes and the design guideline obtained for this scenario also holds for the case of n multiplexing nodes, where $n < N$, since the decoding signal receives the most severe interference for the N multiplexing nodes case. The best performance that can be achieved by the BackCom system is that the signals from all the multiplexed BNs are successfully decoded. In other words, the SINR for the i-th strongest signal, denoted SINR_i, is greater than the channel threshold γ, where $i \in [1, N-1]$, and the signal-to-interference (SNR) for the weakest signal, denoted as SNR_N is also higher than γ.

Let us start from the strongest signal and its SINR is given by $\mathsf{SINR}_1 = \frac{P_T \xi_1 r_1^{-2\alpha}}{\sum_{j=2}^{N} P_T \xi_j r_j^{-2\alpha} + \mathcal{N}}$, where r_j represents the random distance between the reader and the BN from the j-th subregion and its conditional probability density function (PDF) is $f_{r_j}(r_j) = \frac{2r_j}{R_{j+1}^2 - R_j^2}$ with $r_j \in [R_j, R_{j+1}]$. In order to ensure that the strongest signal will always be successfully decoded, the worst case of SINR_1 should always be greater than γ. The worst case for SINR_1 is that $r_1 = R_2$ and $r_j = R_j$; hence, we can write the condition that the strongest signal is always successfully decoded as $\frac{P_T \xi_1 R_2^{-2\alpha}}{\sum_{j=2}^{N} P_T \xi_j R_j^{-2\alpha} + \mathcal{N}} \geq \gamma$. After rearranging the inequality, we obtain $\xi_1 \geq \gamma\left(\sum_{j=2}^{N} \xi_j \frac{R_2^{2\alpha}}{R_j^{2\alpha}} + \frac{\mathcal{N} R_2^{2\alpha}}{P_T}\right)$. Adopting the same procedure, we can find the value of ξ_i for the other signals. ∎

Remark 1: Under the proposed selection criterion, every BN can be successfully decoded for the fading-free scenario. Clearly, when more BNs can be multiplexed (i.e., N is a relatively large value), the network performance can be greatly improved. From (2), we can see that ξ_i is the summation of ξ_j, where $j > i$, and also depends on γ. When γ is large, the obtained ξ_i can be greater than one, which is impractical. In order to meet the condition in (2), we have to set ξ_N as small as possible. Therefore, a natural way of optimally setting the reflection coefficients is to have equality (instead of inequality) in (1) and (2). Note that the transmit power of the reader, P_T, also needs to be sufficiently large when N is large, in order to keep all designed reflection coefficients at the BNs feasible.

IV. Analysis of the Proposed BackCom System with NOMA

In this section, we present the analysis of the performance metrics for our considered BackCom system with NOMA, under the fading-free scenario.

A. Performance Metrics

The *average number of successfully decoded bits*, $\bar{\mathcal{C}}_{\text{suc}}$, is the main metric considered in this work. It is defined as the average number of bits that can be successfully decoded at the reader in one time slot. For a BN, its data bits are said to be successfully decoded if and only if its SINR or SNR is above the threshold. For the system where the coverage region is divided into N subregions, this metric depends on: (i) the average number of successful BNs given that n (where $n \in [1, N]$) BNs are multiplexed, denoted as $\bar{\mathcal{M}}_n$; and (ii) all possible multiplexing scenarios (i.e., the number of BNs in each separate subregion).

For $N = 2$, we investigate the average number of successfully decoded bits, $\bar{\mathcal{C}}_{\text{suc}}$. When $N \geq 3$, there is no general expression for $\bar{\mathcal{C}}_{\text{suc}}$, because the second condition corresponds to the classical balls into bins problem and currently the general form listing all possible allocation cases is not possible [30]. In this work, for $N \geq 3$ scenario, we consider the metric $\bar{\mathcal{M}}_N$, i.e., the average number of successful BNs given N multiplexing nodes. As will be shown in Section VI, $\bar{\mathcal{M}}_N$ has similar trends as $\bar{\mathcal{C}}_{\text{suc}}$ for general N case.

B. Two-Node Pairing Case ($N = 2$)

We first consider the two-node pairing case, which is widely adopted and considered in the NOMA literature due to its feasibility in practical implementation. The definition and the essential expression of $\bar{\mathcal{C}}_{\text{suc}}$ are given below, where the factors used to calculate this metric for different scenarios are summarized in Table I (cf. Section V-C).

Definition 1: Based on our NOMA-enhanced BackCom system in Section II-D, the average number of successfully decoded bits $\bar{\mathcal{C}}_{\text{suc}}$ is

$$\begin{aligned}\bar{\mathcal{C}}_{\text{suc}} =& \sum_{t=0}^{M/2} \binom{t}{M} p_{\text{near}}^t (1-p_{\text{near}})^{M-t} \Bigg(t\frac{2\mathcal{L}\mathcal{R}}{M}\bar{\mathcal{M}}_2 + (M-2t) \\ & \times \frac{\mathcal{L}\mathcal{R}}{M}\bar{\mathcal{M}}_{1\text{near}} \Bigg) + \sum_{t=M/2+1}^{M} \binom{t}{M} p_{\text{near}}^t (1-p_{\text{near}})^{M-t} \\ & \times \left((M-t)\frac{2\mathcal{L}\mathcal{R}}{M}\bar{\mathcal{M}}_2 + (2t-M)\frac{\mathcal{L}\mathcal{R}}{M}\bar{\mathcal{M}}_{1\text{far}} \right), \end{aligned} \tag{3}$$

where p_{near} is the average probability that a BN is residing in the near subregion (i.e., the first subregion) and it equals to $p_{\text{near}} = \frac{R_2^2 - R_1^2}{R^2 - R_1^2}$. $\bar{\mathcal{M}}_{1\text{near}}$ ($\bar{\mathcal{M}}_{1\text{far}}$) denotes the average number of successful BNs coming from the near (far) subregion, given that it accesses the reader alone. $\bar{\mathcal{M}}_2$ is the average number of successful BNs when two BNs are paired, and it can be expressed as $\bar{\mathcal{M}}_2 = p_1 + 2p_2$, where p_2 is the average probability that signals for the paired BNs are successfully decoded and p_1 is the probability that only the stronger signal is successfully decoded.

The key elements that determine $\bar{\mathcal{C}}_{\text{suc}}$ are presented in the following lemmas.

Lemma 1: Based on our system model in Section II, given that two BNs are paired, the probability that the signals from the two BNs are successfully decoded and the probability that the signal from only one BN

This article has been accepted for publication in a future issue of this journal, but has not been fully edited. Content may change prior to final publication. Citation information: DOI 10.1109/TWC.2018.2864741, IEEE Transactions on Wireless Communications

$$p_2=\begin{cases}0, & \left(\gamma\geq\frac{P_T\xi_2R_2^{-2\alpha}}{\mathcal{N}}\right)\,||\,\left(\left(\gamma<\frac{P_T\xi_2R_2^{-2\alpha}}{\mathcal{N}}\right)\,\&\&\,\left(R_1^{-2\alpha}\leq\frac{\mathcal{N}\gamma}{\xi_1P_T}+\max\left\{\frac{1}{R^{2\alpha}},\frac{\mathcal{N}\gamma}{\xi_2P_T}\right\}\gamma\kappa\right)\right);\\ \frac{\left(\max\left\{\frac{1}{R^{2\alpha}},\frac{\mathcal{N}\gamma}{\xi_2P_T}\right\}\right)^{-\frac{1}{\alpha}}-R_2^2}{R^2-R_2^2}, & \left(\gamma<\frac{P_T\xi_2R_2^{-2\alpha}}{\mathcal{N}}\right)\,\&\&\,\left(\gamma\leq\frac{R_2^{-2\alpha}}{\kappa R_2^{-2\alpha}+\frac{\mathcal{N}}{\xi_1P_T}}\right);\\ \Omega\left(\max\left\{\frac{1}{R^{2\alpha}},\frac{R_2^{-2\alpha}}{\gamma\kappa}-\frac{\mathcal{N}}{\xi_2P_T},\frac{\mathcal{N}\gamma}{\xi_2P_T}\right\},\min\left\{\frac{1}{R_2^{2\alpha}},\frac{R_1^{-2\alpha}}{\gamma\kappa}-\frac{\mathcal{N}}{\xi_2P_T}\right\},\max\left\{\frac{1}{R^{2\alpha}},\frac{\mathcal{N}\gamma}{\xi_2P_T}\right\}\right), & \text{otherwise;}\end{cases}\tag{4}$$

$$p_1=\begin{cases}0, & \left(\gamma\leq\frac{P_T\xi_2R^{-2\alpha}}{\mathcal{N}}\right)\,||\,\left(\left(\gamma>\frac{P_T\xi_2R^{-2\alpha}}{\mathcal{N}}\right)\,\&\&\,\left(\gamma\leq\frac{R_1^{-2\alpha}}{\kappa R^{-2\alpha}+\frac{\mathcal{N}}{\xi_1P_T}}\right)\right);\\ \frac{R^2-\left(\min\left\{\frac{1}{R_2^{2\alpha}},\frac{\mathcal{N}\gamma}{\xi_2P_T}\right\}\right)^{-\frac{1}{\alpha}}}{R^2-R_2^2}, & \left(\gamma>\frac{P_T\xi_2R^{-2\alpha}}{\mathcal{N}}\right)\,\&\&\,\left(R_2^{-2\alpha}\geq\frac{\mathcal{N}\gamma}{\xi_1P_T}+\min\left\{\frac{1}{R_2^{2\alpha}},\frac{\mathcal{N}\gamma}{\xi_2P_T}\right\}\gamma\kappa\right);\\ \Omega\left(\max\left\{\frac{1}{R^{2\alpha}},\frac{R_2^{-2\alpha}}{\gamma\kappa}-\frac{\mathcal{N}}{\xi_2P_T}\right\},\min\left\{\frac{1}{R_2^{2\alpha}},\frac{R_1^{-2\alpha}}{\gamma\kappa}-\frac{\mathcal{N}}{\xi_2P_T},\frac{\mathcal{N}\gamma}{\xi_2P_T}\right\},R^{-2\alpha}\right), & \text{otherwise;}\end{cases}\tag{5}$$

is successfully decoded are given by (4) and (5) at the top of this page, respectively, where $\Omega(p,q,w)\triangleq\frac{\left(\frac{P_T\xi_1}{\mathcal{N}\gamma p}\right)^{\frac{1}{\alpha}}{}_2F_1\left[-\frac{1}{\alpha},\frac{1}{\alpha},\frac{\alpha-1}{\alpha},-\frac{P_T\xi_2}{\mathcal{N}}p\right]+q^{-\frac{1}{\alpha}}R_1^{-p^{-\frac{1}{\alpha}}}R_1^2}{(R_2^2-R_1^2)(R^2-R_2^2)}-\frac{w^{-\frac{1}{\alpha}}-p^{-\frac{1}{\alpha}}}{R^2-R_2^2}-\frac{\left(\frac{P_T\xi_1}{\mathcal{N}\gamma q}\right)^{\frac{1}{\alpha}}{}_2F_1\left[-\frac{1}{\alpha},\frac{1}{\alpha},\frac{\alpha-1}{\alpha},-\frac{P_T\xi_2}{\mathcal{N}}q\right]}{(R_2^2-R_1^2)(R^2-R_2^2)}$ and $\kappa\triangleq\frac{\xi_2}{\xi_1}$.

Proof: See Appendix A.

Lemma 2: Based on our system model in Section II, given that only one BN from the near subregion accesses the reader, the average number of successful BNs is

$$\bar{\mathcal{M}}_{1\text{near}}=\frac{\min\left\{R_2^2,\left(\frac{P_T\xi_1}{\gamma\mathcal{N}}\right)^{\frac{1}{\alpha}}\right\}-R_1^2}{R_2^2-R_1^2}\mathbf{1}\left(\frac{P_T\xi_1}{\mathcal{N}R_1^{2\alpha}}\geq\gamma\right),\tag{6}$$

and the average number of successful BNs when only one BN from the far subregion accesses the reader is

$$\bar{\mathcal{M}}_{1\text{far}}=\frac{\min\left\{R^2,\left(\frac{P_T\xi_2}{\gamma\mathcal{N}}\right)^{\frac{1}{\alpha}}\right\}-R_2^2}{R^2-R_2^2}\mathbf{1}\left(\frac{P_T\xi_2}{\mathcal{N}R_2^{2\alpha}}\geq\gamma\right).\tag{7}$$

Proof: From the definition of $\bar{\mathcal{M}}_{1\text{near}}$, it is expressed as $\bar{\mathcal{M}}_{1\text{near}}=\mathbb{E}_{r_1}\left[\Pr\left(\frac{P_T\xi_1r_1^{-2\alpha}}{\mathcal{N}}\geq\gamma\right)\right]$. After rearranging and evaluating this expression, we arrive at the result in (6). ■

Remark 2: Under the selection criterion of the reflection coefficient proposed in Proposition 1, it is clear that $\bar{\mathcal{M}}_2=2$ and $\bar{\mathcal{M}}_{1\text{near}}=\bar{\mathcal{M}}_{1\text{far}}=1$. Consequently, $\bar{\mathcal{C}}_{\text{suc}}$ can be simplified into $\bar{\mathcal{C}}_{\text{suc}}=\mathcal{LR}(1+2p_{\text{near}})+\frac{4\mathcal{LR}p_{\text{near}}^{(M+2)/2}(p_{\text{near}}-1)\binom{M}{(M+2)/2}{}_2F_1\left[1,\frac{2-M}{2},\frac{4+M}{2},\frac{p_{\text{near}}}{p_{\text{near}}-1}\right]}{M(1-p_{\text{near}})^{(4-M)/2}}-\frac{4\mathcal{LR}p_{\text{near}}^{(M+2)/2}p_{\text{near}}\binom{M}{(M+4)/2}{}_2F_1\left[2,\frac{4-M}{2},\frac{6+M}{2},\frac{p_{\text{near}}}{p_{\text{near}}-1}\right]}{M(1-p_{\text{near}})^{(4-M)/2}}$, which is the same as the total number of bits transmitted by BNs. Note that this quantity strongly relies on the radius R_2. The impact of R_2 will be presented in Section VI-D.

Note that, when we set $\xi_2\geq\gamma\frac{\mathcal{N}R^{2\alpha}}{P_T}$, the average number of successful BNs is $\bar{\mathcal{M}}_{\text{suc}}=2p_2$, which is directly proportional to p_2. The closed-form expression shown in (4) involves the hypergeometric function coming from the noise term in the SINR, which makes it generally difficult to obtain any design intuition. By assuming that the noise is negligible, we obtain the following simplified asymptotic result for $\bar{\mathcal{M}}_2$ as

$$\lim_{\mathcal{N}\to0}\bar{\mathcal{M}}_2=\begin{cases}2, & \gamma\kappa\leq1;\\ \frac{2R_2^2R^2+2R_1^2R_2^2-2R_1^2R^2-R_2^4\left((\gamma\kappa)^{-\frac{1}{\alpha}}+(\gamma\kappa)^{\frac{1}{\alpha}}\right)}{2(R_2^2-R_1^2)(R^2-R_2^2)}, & 1<\gamma\kappa\leq\frac{R_2^{-2\alpha}}{R^{-2\alpha}};\\ \frac{2R_1^2R_2^2-2R_1^2R^2+(R^4-R_2^4)(\gamma\kappa)^{\frac{1}{\alpha}}}{2(R_2^2-R_1^2)(R^2-R_2^2)}, & \frac{R_2^{-2\alpha}}{R^{-2\alpha}}<\gamma\kappa\leq\frac{R_1^{-2\alpha}}{R_2^{-2\alpha}};\\ \frac{-2R_1^2R^2+R^4(\gamma\kappa)^{-\frac{1}{\alpha}}+R_1^4(\gamma\kappa)^{\frac{1}{\alpha}}}{2(R_2^2-R_1^2)(R^2-R_2^2)}, & \frac{R_1^{-2\alpha}}{R_2^{-2\alpha}}<\gamma\kappa\leq\frac{R_1^{-2\alpha}}{R^{-2\alpha}};\\ 0, & \gamma\kappa>\frac{R_1^{-2\alpha}}{R^{-2\alpha}}.\end{cases}\tag{8}$$

Remark 3: According to (8), for the given spatial and channel model, $\bar{\mathcal{M}}_2$ is totally determined by the ratio of reflection coefficients κ and the threshold γ. It can be easily proved that the asymptotic result of $\bar{\mathcal{M}}_2$ is a monotonic decreasing function of the γ and κ. Thus, when $\gamma\kappa\leq1$, $\bar{\mathcal{M}}_2$ is maximized. In other words, for the given channel threshold γ, $\kappa=\xi_2/\xi_1$ should be lower than $1/\gamma$ to optimize the network work performance, which is consistent with Proposition 1.

C. Multiple-Node Multiplexing Case ($N\geq3$)

Under this scenario, we analyze the average number of successful BNs given N multiplexing BNs.

Definition 2: Based on our NOMA-enhanced BackCom system in Section II-D, the average number of successful BNs given N multiplexing nodes, $\bar{\mathcal{M}}_N$, is given by

$$\bar{\mathcal{M}}_N=\sum_{k=0}^{N}kp_k,\tag{9}$$

where p_k is the probability that only the signals from the first k BNs are successfully decoded.

The derivation of probability p_k is very challenging. This is because the event that the signal from a BN in i-th subregion is successfully decoded is correlated with the event that the signal from the BN in the $i+1$-th subregion is unsuccessfully decoded. Thus, for analytical tractability, similar to most literatures [17], [29], we assume that each decoding step

This article has been accepted for publication in a future issue of this journal, but has not been fully edited. Content may change prior to final publication. Citation information: DOI 10.1109/TWC.2018.2864741, IEEE Transactions on Wireless Communications

$$\mathcal{M}_{w_i}(s)=\mathbb{E}_{r_i,\ldots,r_N}\left[\exp\left(-\frac{sr_i^{2\alpha}\mathcal{N}}{P_T\xi_i}-\sum_{j=i+1}^{N}sr_i^{2\alpha}r_j^{-\alpha}\frac{\xi_j}{\xi_i}\right)\right]=\mathbb{E}_{r_i}\left[\exp\left(-\frac{sr_i^{2\alpha}\mathcal{N}}{P_T\xi_i}\right)\prod_{j=i+1}^{N}\int_{R_j}^{R_{j+1}}\frac{\exp\left(-sr_i^{2\alpha}r_j^{-\alpha}\frac{\xi_j}{\xi_i}\right)2r_j}{R_{j+1}^2-R_j^2}\mathrm{d}r_j\right]$$
$$=\mathbb{E}_{r_i}\left[\exp\left(-\frac{sr_i^{2\alpha}\mathcal{N}}{P_T\xi_i}\right)\prod_{j=i+1}^{N}\frac{\left(sr_i^{2\alpha}\xi_j/\xi_i\right)^{\frac{1}{\alpha}}}{\alpha(R_{j+1}^2-R_j^2)}\Gamma\left[-\frac{1}{\alpha},sr_i^{2\alpha}\frac{\xi_j}{\xi_iR_{j+1}^{2\alpha}},sr_i^{2\alpha}\frac{\xi_j}{\xi_iR_j^{2\alpha}}\right]\right]. \quad (13)$$

in the SIC is independent. We will show in Section VI that the independence assumption does not adversely affect the accuracy of the analysis. Based on this independence assumption, we can approximately express p_k as

$$p_k\approx p_{\text{out}}^{(k+1)}\prod_{i=1}^{k}\left(1-p_{\text{out}}^{(i)}\right), \quad (10)$$

where $p_{\text{out}}^{(i)}$ denotes the probability when the SINR of the i-th strongest signal (e.g., the signal from the BN in the i-th subregion) falls below γ given that the $i-1$-th strongest signal is successfully decoded. Note that except $p_{\text{out}}^{(1)}$, any $p_{\text{out}}^{(i)}$ is the conditional outage probability.

Different from the previous two-node pairing scenario, there is no direct way to compute $p_{\text{out}}^{(i)}$ when $N>3$. Instead, we adopt the moment generating function (MGF)-based approach in [31] to work out $p_{\text{out}}^{(i)}$, which is presented in the following lemma.

Lemma 3: Based on our system model considered in Section II, the probability that the signal from the i-th BN fails to be decoded, given that the $i-1$-th strongest signal is successfully decoded, is

$$p_{\text{out}}^{(i)}=1-\frac{\exp(\frac{\mathcal{A}}{2})}{2^{\mathcal{B}}\gamma^{-1}}\sum_{b=0}^{\mathcal{B}}\binom{\mathcal{B}}{b}\sum_{c=0}^{\mathcal{C}+b}\frac{(-1)^c}{\mathcal{D}_c}\mathrm{Re}\left\{\frac{\mathcal{M}_{w_i}(s)}{s}\right\}, \quad (11)$$

where $\mathcal{M}_{w_i}(s)=\int_{R_i}^{R_{i+1}}\exp\left(\frac{-sr_i^{2\alpha}\mathcal{N}}{P_T\xi_i}\right)\prod_{j=i+1}^{N}\frac{\left(sr_i^{2\alpha}\frac{\xi_j}{\xi_i}\right)^{\frac{1}{\alpha}}}{\alpha(R_{j+1}^2-R_j^2)}\times\Gamma\left[-\frac{1}{\alpha},\frac{sr_i^{2\alpha}\xi_j}{\xi_iR_{j+1}^{2\alpha}},\frac{sr_i^{2\alpha}\xi_j}{\xi_iR_j^{2\alpha}}\right]\frac{2r_i}{R_{i+1}^2-R_i^2}\mathrm{d}r_i$. $\mathcal{D}_c=2$ (if $c=0$) and $\mathcal{D}_c=1$ (if $c=1,2,\ldots$), $s=(\mathcal{A}+\mathbf{i}2\pi c)/(2\gamma^{-1})$. $\mathcal{A}$, $\mathcal{B}$ and $\mathcal{C}$ are three parameters employed to control the error estimation and following [31], we set $\mathcal{A}=8\ln 10$, $\mathcal{B}=11$, $\mathcal{C}=14$ in this work.

Proof: Based on the MGF-approach, we have $p_{\text{out}}^{(i)}$ as

$$p_{\text{out}}^{(i)}=\Pr\left(\mathsf{SINR}_i<\gamma\right)=\Pr\left(\frac{P_T\xi_ir_i^{-2\alpha}}{\sum_{j=i+1}^{N}P_T\xi_jr_j^{-2\alpha}+\mathcal{N}}<\gamma\right)$$
$$=1-\frac{\exp(\frac{\mathcal{A}}{2})}{2^{\mathcal{B}}\gamma^{-1}}\sum_{b=0}^{\mathcal{B}}\binom{\mathcal{B}}{b}\sum_{c=0}^{\mathcal{C}+b}\frac{(-1)^c}{\mathcal{D}_c}\mathrm{Re}\left\{\frac{\mathcal{M}_{w_i}(s)}{s}\right\}, \quad (12)$$

where w_i is the inverse SINR_i and $\mathcal{M}_{w_i}(s)$ is its distribution's MGF. Following the definition of MGF, we then can express the MGF of the distribution of w_i as (13), at the top of this page. ■

V. Two-Node Pairing Case with Fading

In the previous sections, we investigated the system performance for multiple-node multiplexing scenario under fading-free channel model. In this section, we take the fading channel into account and focus on the analysis for two-node pairing scenario.

The block fading is assumed, which indicates that the fading coefficient is unchanged within one time slot, but it may vary independently from one time slot to another time slot. The fading on the communication link is assumed to be the i.i.d. Nakagami-m fading and let g denote the fading power gain on the communication link that follows gamma distribution. Note that Nakagami-m fading is widely adopted in the literature to model various fading scenarios [31]. By proper parameter mapping, Nakagami-m fading can closely approximate Rician fading, which is used to model the LOS environment. Nagakami-m fading reduces to Rayleigh fading by setting $m=1$. In addition, Nakagami-m fading allows tractability in the analysis. Hence, it is considered in this work. Moreover, we assume that the downlink and uplink channels are reciprocal (i.e., the fading coefficient of the downlink channel is the transpose conjugate of the uplink channel and their fading amplitudes are the same) [11].

When fading is included, another type of randomness is added to the received signal. In this section, we consider two pairing approaches for power-domain NOMA, which are named as the region division and power division, respectively. Under the region division approach, the situation is similar to Section IV-B, where the reader pairs the BNs from the near subregion and far subregion. In the fading context, this approach requires the long term training (i.e., obtaining the long-term average received signal strength) to recognize the BNs either in the near subregion or in the far subregion. In terms of the power division approach, the reader pairs the BNs with the higher instantaneous backscattered power and the lower instantaneous backscattered power, which is based on the instantaneous training to classify the BNs. Its explicit implementation will be explained in Section V-B. Note these two approaches converge to the same one for the fading-free scenario.

The average number of successfully decoded bits, $\bar{\mathcal{C}}_{\text{suc}}$, is the metric investigated under the fading case. Its general expression is the same as (3) in Definition 1 for both approaches, while the key factors, such as p_{near}, p_1, p_2, $\bar{\mathcal{M}}_{1\text{near}}$ and $\bar{\mathcal{M}}_{1\text{far}}$, are changed. The analysis for these factors are presented as follows and the summary is presented in Table I (cf. Section V-C).

A. Region Division Approach

For the region division approach, p_{near} is the probability that the BN is located in the near subregion, which is the same as Section IV-B and is equal to $p_{\text{near}}=\frac{R_2^2-R_1^2}{R^2-R_1^2}$. The

This article has been accepted for publication in a future issue of this journal, but has not been fully edited. Content may change prior to final publication. Citation information: DOI 10.1109/TWC.2018.2864741, IEEE Transactions on Wireless Communications

$$p_2=\begin{cases}\int_{\frac{\mathcal{N}\gamma}{P_T\xi_2(1-\gamma)}}^{\infty}\left(1-\Phi^A(\kappa x_2)\right)\phi^B(x_2)\mathrm{d}x_2+\int_{\frac{\mathcal{N}\gamma}{P_T\xi_2}}^{\frac{\mathcal{N}\gamma}{P_T\xi_2(1-\gamma)}}\left(1-\Phi^A\left(\gamma\kappa x_2+\frac{\mathcal{N}\gamma}{P_T\xi_1}\right)\right)\phi^B(x_2)\mathrm{d}x_2 \\ +\int_{\frac{\mathcal{N}\gamma}{P_T\xi_1(1-\gamma)}}^{\infty}\left(1-\Phi^B\left(\frac{x_1}{\kappa}\right)\right)\phi^A(x_1)\mathrm{d}x_1+\int_{\frac{\mathcal{N}\gamma}{P_T\xi_1}}^{\frac{\mathcal{N}\gamma}{P_T\xi_1(1-\gamma)}}\left(1-\Phi^B\left(\frac{\gamma x_1}{\kappa}+\frac{\mathcal{N}\gamma}{P_T\xi_2}\right)\right)\phi^A(x_1)\mathrm{d}x_1, & \gamma<1; \\ \int_{\frac{\mathcal{N}\gamma}{P_T\xi_2}}^{\infty}\left(1-\Phi^A\left(\gamma\kappa x_2+\frac{\mathcal{N}\gamma}{P_T\xi_1}\right)\right)\phi^B(x_2)\mathrm{d}x_2+\int_{\frac{\mathcal{N}\gamma}{P_T\xi_1}}^{\infty}\left(1-\Phi^B\left(\frac{\gamma x_1}{\kappa}+\frac{\mathcal{N}\gamma}{P_T\xi_2}\right)\right)\phi^A(x_1)\mathrm{d}x_1, & \gamma\geq 1;\end{cases} \tag{17}$$

$$p_1=\int_0^{\frac{\mathcal{N}\gamma}{P_T\xi_2}}\left(1-\Phi^A\left(\gamma\kappa x_2+\frac{\mathcal{N}\gamma}{P_T\xi_1}\right)\right)\phi^B(x_2)\mathrm{d}x_2+\int_0^{\frac{\mathcal{N}\gamma}{P_T\xi_1}}\left(1-\Phi^B\left(\frac{\gamma x_1}{\kappa}+\frac{\mathcal{N}\gamma}{P_T\xi_2}\right)\right)\phi^A(x_1)\mathrm{d}x_1. \tag{18}$$

$$\begin{aligned}p_2=&\underbrace{\Pr\left(\frac{P_T\xi_1g_1^2r_1^{-2\alpha}}{P_T\xi_2g_2^2r_2^{-2\alpha}+\mathcal{N}}\geq\gamma\ \&\&\ \frac{P_T\xi_2g_2^2r_2^{-2\alpha}}{\mathcal{N}}\geq\gamma\ \&\&\ \frac{\xi_1g_1^2}{r_1^{2\alpha}}\geq\frac{\xi_2g_2^2}{r_2^{2\alpha}}\right)}_{p_2^A}\\&+\underbrace{\Pr\left(\frac{P_T\xi_2g_2^2r_2^{-2\alpha}}{P_T\xi_1g_1^2r_1^{-2\alpha}+\mathcal{N}}\geq\gamma\ \&\&\ \frac{P_T\xi_1g_1^2r_1^{-2\alpha}}{\mathcal{N}}\geq\gamma\ \&\&\ \frac{\xi_1g_1^2}{r_1^{2\alpha}}<\frac{\xi_2g_2^2}{r_2^{2\alpha}}\right)}_{p_2^B}.\end{aligned} \tag{19}$$

analysis of p_k (i.e., the probability that the signals from k BNs are successfully decoded) becomes complicated due to the consideration of fading.

Note that our considered SIC scheme is based on the instantaneous received power at the reader, i.e., $P_T\xi g^2r^{-2\alpha}$. Under the region division approach, the stronger signal may not come from the BN in the near subregion. Before deriving p_k, we first present the following lemma which shows the composite distribution of the random distance and fading.

Lemma 4: Let r denote a random variable following the distribution of $f_r(r)=\frac{2r}{R_u^2-R_l^2}$, where $r\in[R_l,R_u]$, and g is a random variable following the gamma distribution, i.e., $f_g(g)=\frac{m^mg^{m-1}\exp(-mg)}{\Gamma[m]}$. The cumulative distribution function (CDF) and PDF for the composite random variable $x\triangleq g^2r^{-2\alpha}$ are given by

$$\begin{aligned}\Phi(x,R_l,R_u)=&1-\frac{\Gamma\left[m+\frac{2}{\alpha},mR_l^\alpha\sqrt{x},mR_u^\alpha\sqrt{x}\right]}{(m\sqrt{x})^{\frac{2}{\alpha}}\left(R_u^2-R_l^2\right)\Gamma[m]}\\&+\frac{R_l^2\Gamma[m,mR_l^\alpha\sqrt{x}]-R_u^2\Gamma[m,mR_u^\alpha\sqrt{x}]}{\left(R_u^2-R_l^2\right)\Gamma[m]},\end{aligned} \tag{14}$$

$$\phi(x,R_l,R_u)=\frac{\Gamma\left[m+\frac{2}{\alpha},mR_l^\alpha\sqrt{x},mR_u^\alpha\sqrt{x}\right]}{m^{\frac{2}{\alpha}}x^{\frac{1}{\alpha}+1}\alpha\left(R_u^2-R_l^2\right)\Gamma[m]}, \tag{15}$$

respectively.

Proof: The CDF of x can be written as

$$\begin{aligned}&\Phi(x,R_l,R_u)=\Pr\left(g^2r^{-2\alpha}<x\right)=\mathbb{E}_r\left\{\Pr\left(g<r^\alpha\sqrt{x}\right)\right\}\\&=\int_{R_l}^{R_u}\frac{\Gamma\left[m,0,m\sqrt{x}r^\alpha\right]}{\Gamma[m]}\frac{2r}{R_u^2-R_l^2}\,\mathrm{d}r\\&=1-\frac{\Gamma\left[m+\frac{2}{\alpha},mR_l^\alpha\sqrt{x},mR_u^\alpha\sqrt{x}\right]}{(m\sqrt{x})^{\frac{2}{\alpha}}\left(R_u^2-R_l^2\right)\Gamma[m]}\\&+\frac{R_l^2\Gamma[m,mR_l^\alpha\sqrt{x}]-R_u^2\Gamma[m,mR_u^\alpha\sqrt{x}]}{\left(R_u^2-R_l^2\right)\Gamma[m]}.\end{aligned} \tag{16}$$

Taking the derivative of $\Phi(x,R_l,R_u)$ with respect to x, we obtain its PDF. ■

According to Lemma 4 and probability theory, the key elements for the region division approach with fading are shown in the following lemmas.

Lemma 5: Based on our system model considered in Sections II and V, under the fading scenario with region division approach, the probability that the signals from two BNs are successfully decoded and the probability that the signal from only one BN is successfully decoded are given by (17) and (18) at the top of this page, respectively, where $\kappa=\xi_2/\xi_1$, $\Phi^A(x_1)\triangleq\Phi(x_1,R_1,R_2)$, $\phi^A(x_1)\triangleq\phi(x_1,R_1,R_2)$, $\Phi^B(x_2)\triangleq\Phi(x_2,R_2,R)$ and $\phi^B(x_2)\triangleq\phi(x_2,R_2,R)$. $\Phi(\cdot,\cdot,\cdot)$ and $\phi(\cdot,\cdot,\cdot)$ are defined in Lemma 4.

Proof: In order to ensure that the signals from both paired BNs are successfully decoded, it requires both of the SINR from the stronger signal and the SNR from the weaker signal to be greater than the channel threshold. Based on the decoding order, p_2 can be decomposed into (19) at the top of this page, where $x_1\triangleq r_1^{2\alpha}/g_1^2$, $x_2\triangleq r_2^{2\alpha}/g_2^2$, g_1 and g_2 represent the fading power gain for the BN from the near subregion and far subregion, respectively.

Let us consider p_2^A firstly, which is the probability that both BNs are successfully decoded when the signal from the near BN is decoded at first. The condition of the signal from the near BN being decoded at first is $\xi_1x_1\geq\xi_2x_2$ (equivalently, $x_1\geq\kappa x_2$). Additionally, the condition that the signal from the far BN is successfully decoded is that x_2 must be greater than $\frac{\mathcal{N}\gamma}{P_T\xi_2}$. Then, we can express p_2^A as

$$\begin{aligned}p_2^A&=\Pr\left(\frac{x_1}{\kappa x_2+\frac{\mathcal{N}}{P_T\xi_1}}\geq\gamma\right)\\&=\mathbb{E}_{x_2}\left\{\Pr\left(x_1\geq\gamma\kappa x_2+\frac{\mathcal{N}\gamma}{P_T\xi_1}\right)\right\},\end{aligned} \tag{20}$$

This article has been accepted for publication in a future issue of this journal, but has not been fully edited. Content may change prior to final publication. Citation information: DOI 10.1109/TWC.2018.2864741, IEEE Transactions on Wireless Communications

$$p_2=\begin{cases}0, & \tilde{\beta}\le\frac{\mathcal{N}\gamma}{P_T\xi_2};\\ \int_{\min\left\{\tilde{\beta},\max\left\{\frac{\mathcal{N}\gamma}{P_T\xi_2},\frac{\tilde{\beta}}{\gamma\kappa}-\frac{\mathcal{N}}{P_T\xi_2}\right\}\right\}}^{\tilde{\beta}}\left(1-\frac{\Phi\left(\gamma\kappa x_2'+\frac{\mathcal{N}\gamma}{P_T\xi_1},R_1,R\right)-\Phi\left(\tilde{\beta},R_1,R\right)}{1-\Phi\left(\tilde{\beta},R_1,R\right)}\right)\frac{\phi\left(x_2',R_1,R\right)}{\Phi\left(\tilde{\beta},R_1,R\right)}\mathrm{d}x_2' & \\ +\frac{\Phi\left(\min\left\{\tilde{\beta},\max\left\{\frac{\mathcal{N}\gamma}{P_T\xi_2},\frac{\tilde{\beta}}{\gamma\kappa}-\frac{\mathcal{N}}{P_T\xi_2}\right\}\right\},R_1,R\right)-\Phi\left(\frac{\mathcal{N}\gamma}{P_T\xi_2},R_1,R\right)}{\Phi\left(\tilde{\beta},R_1,R\right)}, & \tilde{\beta}>\frac{\mathcal{N}\gamma}{P_T\xi_2};\end{cases} \tag{23}$$

$$p_1=\int_{\min\left\{\tilde{\beta},\frac{\mathcal{N}\gamma}{P_T\xi_2},\max\left\{0,\frac{\tilde{\beta}}{\gamma\kappa}-\frac{\mathcal{N}}{P_T\xi_2}\right\}\right\}}^{\min\left\{\tilde{\beta},\frac{\mathcal{N}\gamma}{P_T\xi_2}\right\}}\left(1-\frac{\Phi\left(\gamma\kappa x_2'+\frac{\mathcal{N}\gamma}{P_T\xi_1},R_1,R\right)-\Phi\left(\tilde{\beta},R_1,R\right)}{1-\Phi\left(\tilde{\beta},R_1,R\right)}\right)\frac{\phi\left(x_2',R_1,R\right)}{\Phi\left(\tilde{\beta},R_1,R\right)}\mathrm{d}x_2' + \frac{\Phi\left(\min\left\{\tilde{\beta},\frac{\mathcal{N}\gamma}{P_T\xi_2},\max\left\{0,\frac{\tilde{\beta}}{\gamma\kappa}-\frac{\mathcal{N}}{P_T\xi_2}\right\}\right\},R_1,R\right)}{\Phi\left(\tilde{\beta},R_1,R\right)}. \tag{24}$$

where $x_1\in(\kappa x_2,\infty)$ and $x_2\in\left(\frac{\mathcal{N}\gamma}{P_T\xi_2},\infty\right)$.

Then following the similar procedure as presented in Appendix A, we obtain the expression of p_2^A. p_2^B can be derived using the same procedure. After combining these two results, we arrive at the final result in (17). The derivation of p_1 is similar. ∎

Due to the complexity of functions Φ and ϕ, it is not possible to obtain the closed-form results. But the single-fold integration can be easily numerically evaluated using standard mathematical packages such as Mathematica or Matlab.

Lemma 6: Based on our system model considered in Sections II and V, under the fading scenario with region division approach, the average number of successful BNs given that only one BN from the near subregion accesses the reader is

$$\bar{\mathcal{M}}_{\text{1near}}=1-\Phi^A\left(\frac{\mathcal{N}\gamma}{P_T\xi_1}\right), \tag{21}$$

and the average number of successful BNs given that only one BN from the far subregion accesses the reader is

$$\bar{\mathcal{M}}_{\text{1far}}=1-\Phi^B\left(\frac{\mathcal{N}\gamma}{P_T\xi_2}\right). \tag{22}$$

Since the derivation is similar to the proof of Lemma 2, we skip it here for the sake of brevity.

B. Power Division Approach

Under the power division approach, rather than pairing the BNs from different subregions, the reader pairs the BNs with different power levels. Specifically, for the reader, there is a pre-defined threshold β and training period at the start of each time slot. By comparing the threshold β with the instantaneous backscattered signal power from each node, the reader categorizes the BNs into high power level group and low power level group. Correspondingly, each BN can pick its reflection coefficient by comparing its received power with the threshold $(1-\xi_1)\sqrt{P_T\beta/\xi_1}$ [5]. If the received power is greater than the threshold, this BN belongs to the high power level group and its reflection coefficient will be set to ξ_1. Otherwise, it belongs to the low level power level group and the reflection coefficient is set to ξ_2.

[5]In the training period, all the BNs' reflection coefficients are assumed to be ξ_1.

According to the principle of power division approach, p_{near} can be interpreted as the probability that the backscattered signal power for the node is greater than the threshold β. Thus, p_{near} can be written as $p_{\text{near}}=1-\Phi\left(\tilde{\beta},R_1,R\right)$, where $\tilde{\beta}\triangleq\beta/(P_T\xi_1)$ is the normalized threshold. The key results for p_2, p_1, $\bar{\mathcal{M}}_{\text{1near}}$ and $\bar{\mathcal{M}}_{\text{1far}}$ are given in the following lemmas.

Lemma 7: Based on our system model considered in Sections II and V, under the fading scenario with power division approach, the probability that the signals from two BNs are successfully decoded is (23) at the top of this page, and the probability that the signal from only one BN is successfully decoded is given by (24).

Proof: Let x_1' represent the normalized instantaneous received power from a BN belonging to the high power level group, which is normalized over P_T and ξ_1, and its CDF can be expressed as $F_{x_1'}(x_1')=\frac{\Phi\left(x_1',R_1,R\right)-\Phi\left(\tilde{\beta},R_1,R\right)}{1-\Phi\left(\tilde{\beta},R_1,R\right)}$, where $x_1'\in[\tilde{\beta},\infty)$. Similarly, let x_2' denote the normalized instantaneous received power from a BN belonging to the lower power level group and its CDF is $F_{x_2'}(x_2')=\frac{\Phi\left(x_2',R_1,R\right)}{\Phi\left(\tilde{\beta},R_1,R\right)}$, where $x_2'\in(0,\tilde{\beta})$.

Clearly, under the power division approach, the decoding order is always from the high power level group to the low power level group. These two probabilities p_2 and p_1 are then written as $p_2=\mathbb{E}_{x_1',x_2'}\left[\Pr\left(\frac{P_T\xi_1x_1'}{P_T\xi_2x_2'+\mathcal{N}}\ge\gamma\&\&\frac{P_T\xi_2x_2'}{\mathcal{N}}\ge\gamma\right)\right]$ and $p_1=\mathbb{E}_{x_1',x_2'}\left[\Pr\left(\frac{P_T\xi_1x_1'}{P_T\xi_2x_2'+\mathcal{N}}\ge\gamma\&\&\frac{P_T\xi_2x_2'}{\mathcal{N}}<\gamma\right)\right]$, respectively. Following the similar derivation approach in Appendix A, we arrive at the results in (23) and (24). ∎

Lemma 8: Based on our system model considered in Sections II and V, under the fading scenario with power division approach, the average number of successful BNs given that only one BN from the near subregion accesses the reader is

$$\bar{\mathcal{M}}_{\text{1near}}=1-\Phi\left(\frac{\mathcal{N}\gamma}{\xi_1P_T},R_1,R\right)\mathbf{1}\left(\frac{\mathcal{N}\gamma}{\xi_1P_T}>\tilde{\beta}\right), \tag{25}$$

and the average number of successful BNs given that only one BN from the far subregion accesses the reader is

$$\bar{\mathcal{M}}_{\text{1far}}=\left(1-\Phi\left(\frac{\mathcal{N}\gamma}{\xi_2P_T},R_1,R\right)\right)\mathbf{1}\left(\frac{\mathcal{N}\gamma}{\xi_2P_T}<\tilde{\beta}\right). \tag{26}$$

TABLE I
KEY FACTORS DETERMINING $\bar{\mathcal{C}}_{\text{SUC}}$ FOR TWO-NODE PAIRING CASE.

Scenario	p_{near}	p_2	p_1	$\mathcal{M}_{1\text{near}}$	$\mathcal{M}_{1\text{far}}$
Fading-free	$\frac{R_2^2-R_1^2}{R^2-R_1^2}$	(4)	(5)	(6)	(7)
Fading: region division	$\frac{R_2^2-R_1^2}{R^2-R_1^2}$	(17)	(18)	(21)	(22)
Fading: power division	$1-\Phi\left(\tilde{\beta}, R_1, R\right)$	(23)	(24)	(25)	(26)

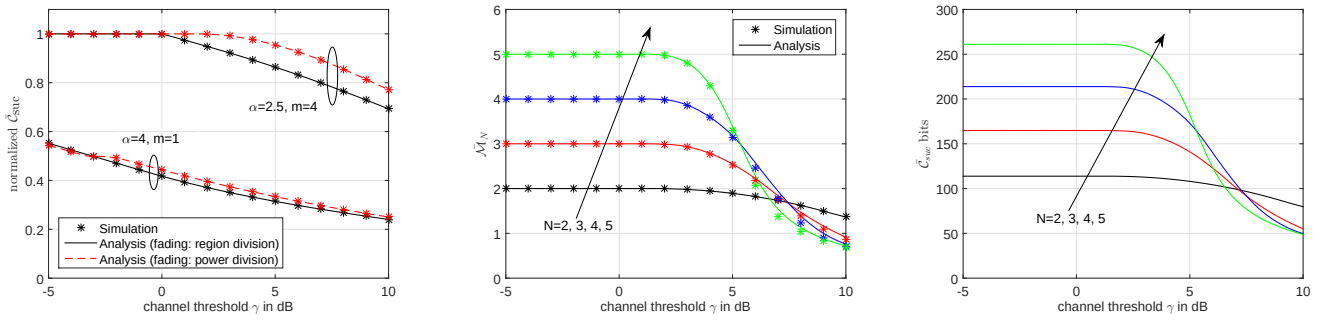

(a) Two-node pairing. (b) Multiple-node multiplexing. (c) Multiple-node multiplexing (simulation only).

Fig. 3. Channel threshold γ versus (a) the normalized average number of successfully decoded bits under two-node pairing; (b) the average number of successful BNs $\bar{\mathcal{M}}_N$ given N multiplexing nodes and (c) the average number of successfully decoded bits $\bar{\mathcal{C}}_{\text{suc}}$ for general multiplexing case.

The derivation is similar to the proof of Lemma 2; hence, we skip it here for the sake of brevity.

Remark 4: The reflection coefficient selection criterion for the region division approach depends on the subregion radius and channel threshold, while the selection criterion for the power division approach strongly relies on the threshold β and channel threshold. Following the same derivation procedure for Proposition 1, to achieve the better system performance, we can compute the relationship between ξ_1 and ξ_2 as

$$\xi_1 \geq \max\left\{\xi_2, \gamma\left(\xi_2 + \frac{\mathcal{N}}{P_T\tilde{\beta}}\right)\right\}. \tag{27}$$

C. Summary

Table I summarizes the key factors used to calculate the average number of successfully decoded bits, $\bar{\mathcal{C}}_{\text{suc}}$, under the fading-free and fading scenarios with different pairing approaches. The general expression of $\bar{\mathcal{C}}_{\text{suc}}$ for two-node pairing is given in (3), where $\bar{\mathcal{M}}_2 = p_1 + 2p_2$.

VI. NUMERICAL RESULTS

In this section, we present the numerical results to investigate the performance of the NOMA-enhanced BackCom system. In order to validate the numerical results, we also present simulation results which are generated using Matlab and are averaged over 10^6 simulation runs. Unless specified otherwise, the following values of the main system parameters are adopted: the outer radius of the coverage zone $R = 65$ m, the inner radius of the coverage zone $R_1 = 1$ m, the number of BNs $M = 60$, the path-loss exponent $\alpha = 2.5$ for Nakagami-m ($m = 4$) fading scenario and fading-free scenario while $\alpha = 4$ for Rayleigh fading case, the reader's transmit power $P_T = 35$ dBm, the noise power $\mathcal{N} = -100$ dBm, and the product of the time slot and the data rate $\mathcal{LR} = 60$ bits. In addition, for the region division approach, we set $R_i = \sqrt{\frac{(i-1)R^2+(N+1-i)R_1^2}{N}}$ for $i = 2, ..., N$. As for the power division approach, we find a $\tilde{\beta}$ value that makes $p_{\text{near}} = 0.5$. Note that such a value ensures that the average number of BNs in each group is the same. The impact of R_2 and $\tilde{\beta}$ will be analyzed in the following Section VI-D.

A. Analysis Validation

Fig. 3 plots the channel threshold γ versus the (normalized) average number of successfully decoded bits $\bar{\mathcal{C}}_{\text{suc}}$ and the average number of successful BNs $\bar{\mathcal{M}}_N$ given N multiplexing nodes for different fading and multiplexing scenarios. Note that the *normalized average number of successfully decoded bits* is defined as the average number of successfully decoded bits over the total number of bits transmitted by BNs, where the latter term is a constant for the given system setup and is given by the formulation in Remark 2. We set $\xi_1 = 0.7$, $\xi_2 = 0.5$, $\xi_3 = 0.3$, $\xi_4 = 0.1$ and $\xi_5 = 0.05$. The curves in Fig. 3(c) are generated using simulations only. From Fig. 3(a) and $N = 2$ curve in Fig. 3(b), we can see that the simulation results match perfectly with the analytical results as expected. As for the $N \geq 3$ curves in Fig. 3(b), we find that, when the channel threshold is large, the analytical results slightly deviate from the simulation results. This is due to the independence assumption we made when calculating p_k for more users multiplexing scenario. The (close) match of the simulation and analytical results demonstrates the accuracy of our derivations. Furthermore, comparing Fig. 3(b) with Fig. 3(c), we find the trends for $\bar{\mathcal{M}}_N$ and $\bar{\mathcal{C}}_{\text{suc}}$ are the same. This indicates that $\bar{\mathcal{M}}_N$ is a reasonable metric to investigate the performance.

As shown in Fig. 3, when the considered reflection coefficient sets satisfy the criteria proposed in Proposition 1 and Remark 4 for certain value of γ, the curves for fading-free and Nakagami fading (i.e., $\alpha = 2.4$, $m = 4$) scenarios are constant. These are the best achievable system performance, where all

This article has been accepted for publication in a future issue of this journal, but has not been fully edited. Content may change prior to final publication. Citation information: DOI 10.1109/TWC.2018.2864741, IEEE Transactions on Wireless Communications

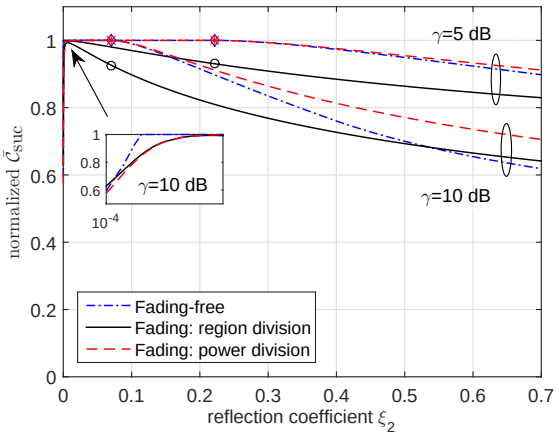

Fig. 4. The reflection coefficient of the far backscatter group ξ_2 versus the normalized average number of successfully decoded bits for two-node pairing.

the transmitted bits are successfully delivered and the average number of successfully decoded bits is the same as the total number of bits transmitted by BNs. Note that the normalized $\bar{C}_{\text{suc}}$ under Rayleigh fading can only achieve about half of the best performance; hence, in the following subsections, we focus on the fading-free and Nakagami fading (i.e., $\alpha = 2.4$, $m = 4$) scenarios.

B. Effect of the Reflection Coefficient for Two-Node Pairing

In this subsection, we investigate the effect of reflection coefficient for the two-node pairing case and examine the proposed reflection coefficient selection criteria. Fig. 4 plots the reflection coefficient of the far backscatter group ξ_2 versus the normalized average number of successfully decoded bits. We set $\xi_1 = 0.7$.

From Fig. 4, we can see that the general trend for the normalized $\bar{C}_{\text{suc}}$ is decreasing as ξ_2 increases. This shows that a smaller value of ξ_2 can benefit the system. This is because, by reducing ξ_2, the interference from the weaker signal is reduced; the stronger signal, thus, has the higher chance to be decoded successfully. However, ξ_2 cannot be set too small, as the curves begin to decrease when ξ_2 approaches to an extremely small value (e.g., 10^{-4}). When ξ_2 is extremely small, the weaker signal is less likely to be decoded successfully (i.e., SNR is very small for most of the time), which leads to the reduction of p_2, $\bar{\mathcal{M}}_2$ and $\bar{C}_{\text{suc}}$ correspondingly.

We also mark the maximum ξ_2 and the corresponding normalized $\bar{C}_{\text{suc}}$ which satisfies (2) or (27) in Fig. 4. We find that, under the fading-free scenario or fading case with the power division approach, the marked normalized $\bar{C}_{\text{suc}}$ is equal to 1, which implies that the signals from all the paired BNs are successfully decoded and the system performance is consequently optimized. It also validates our proposed selection criteria. For the fading case with the region division approach, the proposed selection criterion still provides a good performance (i.e., the marked normalized $\bar{C}_{\text{suc}}$ is 0.9265 for $\gamma = 10$ dB and 0.9306 for $\gamma = 5$ dB).

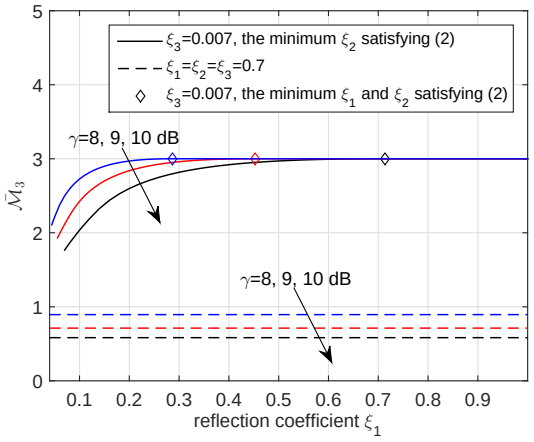

(a) $N = 3$.

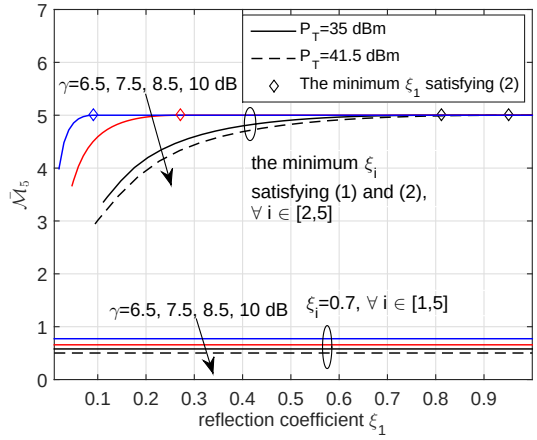

(b) $N = 5$.

Fig. 5. The reflection coefficient of the first backscatter group ξ_1 versus the average number of successful BNs $\bar{\mathcal{M}}_N$ given N multiplexing BNs.

C. Effect of the Reflection Coefficient for Multiple-Node Multiplexing

Fig. 5 plots the reflection coefficient of the first backscatter group ξ_1 versus the average number of successful BNs $\bar{\mathcal{M}}_N$ given N multiplexing BNs, under the fading-free scenario, for $N = 3$ and $N = 5$, respectively. In Fig. 5(a), we set $\xi_3 = 0.007$ and ξ_2 to be the minimum value satisfying (2). In Fig. 5(b), we set ξ_5 to be the minimum value which satisfies (1) and ξ_i (where $i \in [2, 4]$) to be the minimum value satisfying (2). We also mark the minimum ξ_1 satisfying (2). As expected, these curves increase as ξ_1 increases and then become a constant (e.g., $\bar{\mathcal{M}}_N = N$) after the marked points. For the purpose of comparison, we also plot the curves when the reflection coefficients for all the subregions are the same. It is clear that, by properly selecting the reflection coefficients, the performance for BackCom system with NOMA can be greatly enhanced.

In addition, as shown in Fig. 5(b), when $N = 5$ and $P_T = 35$ dBm, the system can achieve the optimum performance when the channel threshold γ is less than 8.5 dB. If γ further increases, the minimum ξ_1 satisfying (2) will be greater than one, which is impossible. Thus, we have to increase the

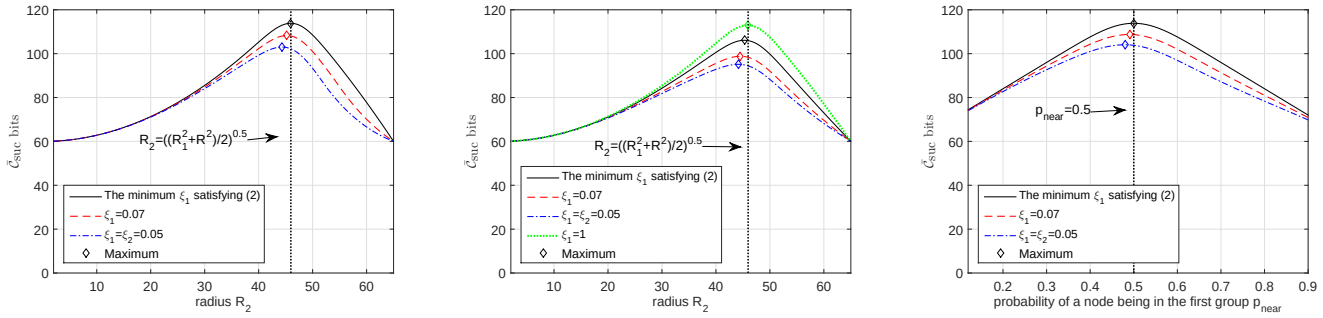

(a) Fading-free scenario. (b) Fading: region division. (c) Fading: power division.

Fig. 6. The average number of successfully decoded bits $\bar{C}_{\text{suc}}$ versus (a) the radius R_2 under fading-free scenario; (b) the radius R_2 with fading and (c) the probability p_{near} with power division approach.

transmit power of the reader in order to set a smaller ξ_5. In Fig. 5(b), we plot the curve for $P_T = 41.5$ dBm, which allows to achieve the best performance when γ is less than 10 dB.

D. Effect of R_2 and $\tilde{\beta}$

In this subsection, we investigate the impact of the radius R_2 for the region division approach and the threshold β for the power division approach. To analyze the impact of system parameters, we focus on the metric $\bar{C}_{\text{suc}}$ rather than the normalized $\bar{C}_{\text{suc}}$, since the total number of bits transmitted by BNs varies for different system setups. Figs. 6(a) and 6(b) plot the radius R_2 versus the average number of successfully decoded bits $\bar{C}_{\text{suc}}$ for fading-free and fading scenarios, respectively. Fig. 6(c) plots the probability p_{near} versus $\bar{C}_{\text{suc}}$ for the fading case with the power division approach. We set channel threshold $\gamma = 5$ dB and $\xi_2 = 0.05$. We also mark the maximum $\bar{C}_{\text{suc}}$ reached by each case. From these figures, we can see that, when p_{near} is varying from 0 to 1 (equivalently, R_2 varies from R_1 to R for the region division approach), $\bar{C}_{\text{suc}}$ first increases and then decreases. When ξ_1 follows the selection criterion in Proposition 1 and Remark 4, the maximum $\bar{C}_{\text{suc}}$ is achieved for $p_{\text{near}} = 0.5$ (equivalently, $R_2 = \sqrt{\frac{R_1^2+R^2}{2}}$ for the region division approach). This is due to the fact that when the reflection coefficients follow the selection criterion in Proposition 1 or Remark 4, $\bar{M}_2$ is always equal to 2 and it is the best performance gain achieved by pairing BNs. Hence, the overall system can benefit more when more BNs are paired. $p_{\text{near}} = 0.5$ can result in the highest probability that all BNs are paired, thereby maximizing the average number of successfully decoded bits $\bar{C}_{\text{suc}}$.

For other scenarios, $p_{\text{near}} = 0.5$ may not lead to the maximum $\bar{C}_{\text{suc}}$. This is because, when $\bar{M}_2$ is no longer equal to 2, both $\bar{M}_2$ and the probability of different pairing cases (equivalently, p_{near}) are determined by R_2 or $\tilde{\beta}$. The varying of R_2 or $\tilde{\beta}$ results in the different value of $\bar{M}_2$ and p_{near}, and the interplay of these two factors results in the different maximum $\bar{C}_{\text{suc}}$ that can be achieved by the system. In addition, we find that the maximum $\bar{C}_{\text{suc}}$ achieved by the system where $\bar{M}_2 < 2$ is always less than the maximum $\bar{C}_{\text{suc}}$ achieved by the system where $\bar{M}_2 = 2$. This shows the importance of carefully selecting system parameters in order to achieve the best performance.

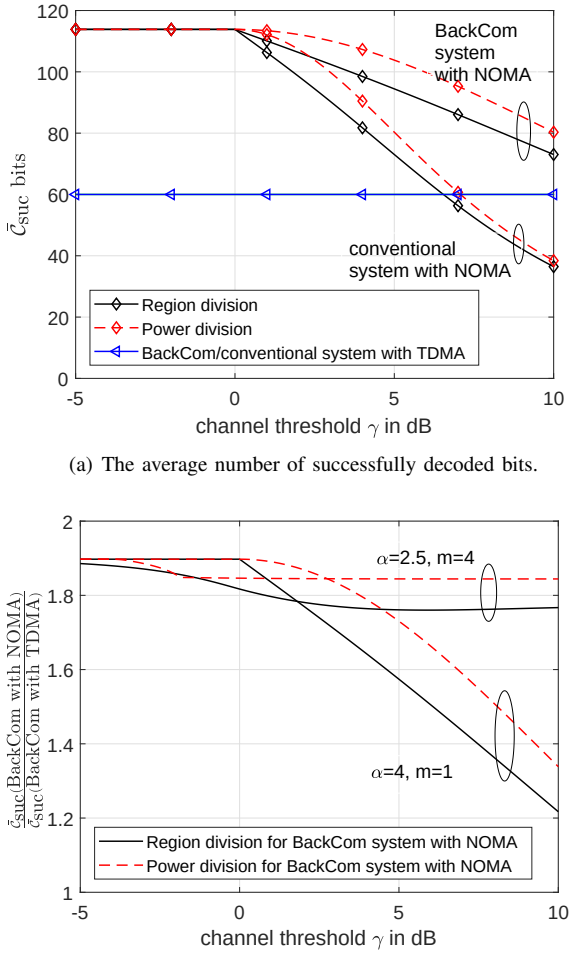

(a) The average number of successfully decoded bits.

(b) The ratio of $\bar{C}_{\text{suc}}$ for BackCom system with/without NOMA.

Fig. 7. Channel threshold γ versus (a) the average number of successfully decoded bits $\bar{C}_{\text{suc}}$ under $\alpha = 2.5$, $m = 4$ and (b) the ratio of $\bar{C}_{\text{suc}}$ for BackCom system with/without NOMA.

E. Performance Gain Achieved by Applying NOMA to the BackCom System

In this subsection, we evaluate the performance gain achieved by adopting NOMA into the BackCom system. We compare our scheme with the following three benchmark

This article has been accepted for publication in a future issue of this journal, but has not been fully edited. Content may change prior to final publication. Citation information: DOI 10.1109/TWC.2018.2864741, IEEE Transactions on Wireless Communications

systems:

- *Conventional communication system with NOMA:* the transmitting nodes are active devices, i.e., they actively transmit signal to the reader and the reader does not transmit the CW signal at all in the uplink communication. The remaining system model is the same as Section II-D (i.e., hybrid of TDMA and NOMA).
- *BackCom system with TDMA:* the transmitting nodes are BNs. Each time slot is divided into M mini-slots each lasting $\frac{\mathcal{L}}{M}$ seconds. Only one BN is scheduled to modulate and backscatter the signal to the reader in each mini-slot.
- *Conventional communication system with TDMA:* the transmitting nodes are active devices. Each time slot is divided into M mini-slots each lasting $\frac{\mathcal{L}}{M}$ seconds. Only one node is scheduled to actively transmit the signal to the reader in each mini-slot.

The analytical results for these benchmark system can be derived using our analysis in this work. For the sake of brevity, we omit them here. Additionally, for a fair comparison among different communication systems, we assume that $\xi = 0.7$ for all BNs and the transmit power for all conventional nodes are set to same, i.e., 20 dBm.

Figs. 7(a) plots the channel threshold γ versus the average number of successfully decoded bits $\bar{\mathcal{C}}_{\text{suc}}$. We first *compare the BackCom system with the conventional system under NOMA scenario*. As shown in this figure, under the good channel condition (i.e., the channel condition tends to be LOS), the BackCom system has the larger average number of successfully decoded bits $\bar{\mathcal{C}}_{\text{suc}}$ than the conventional system. This is mainly caused by the double attenuation of the received power at the reader for the BackCom system. This double attenuation effect can boost the performance of the BackCom system with NOMA under good channel condition. When the channel condition is good, the BNs are very likely to be successfully decoded alone. The double attenuation effect can make the channel gain between the stronger signal and weaker signal more distinguishable; hence, introducing the NOMA (i.e., bringing in the interference from the weaker signal) results in a small impact on the system.

We then *compare the BackCom system with NOMA and the BackCom system with TDMA*, and we also plot the ratio of $\bar{\mathcal{C}}_{\text{suc}}$ for these two systems in Fig. 7(b). From this figure, we can see that the BackCom system with NOMA generally leads to a better performance than the BackCom system with TDMA regardless of channel conditions. Under the case of same reflection coefficient, the system with NOMA allows two BNs to access the reader at the same time, which makes the reader experience the interference from the weaker signal when decoding the stronger signal. Hence, it is possible that less number of BNs can be successfully decoded when BNs are paired. However, in terms of the average number of successfully decoded bits, since the time on each mini-slot under NOMA is doubled, the BackCom system with NOMA can achieve larger $\bar{\mathcal{C}}_{\text{suc}}$ than the system with TDMA. This illustrates why it is beneficial to apply NOMA to the BackCom system. In particular, by setting the proper reflection coefficients for the BackCom system with NOMA, the performance gain can be further improved.

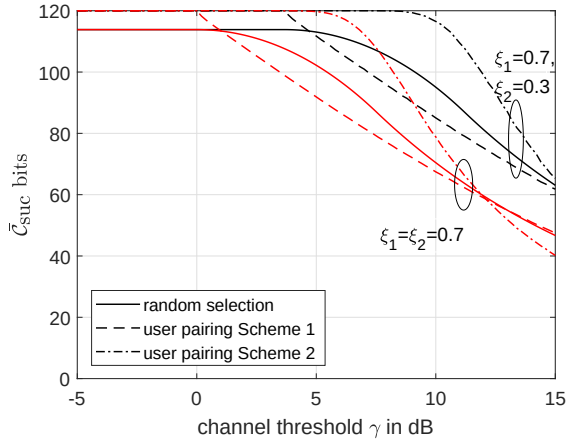

(a) Fading-free Scenario.

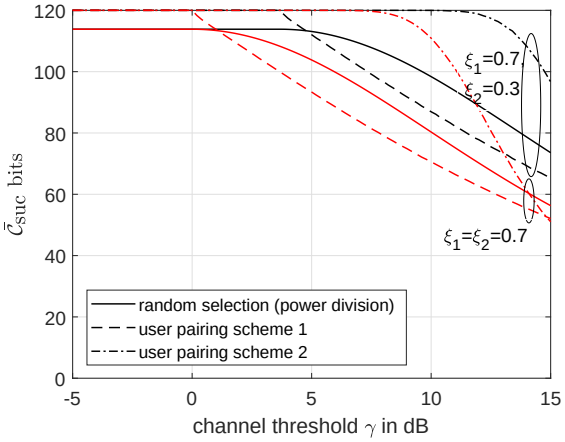

(b) $\alpha = 2.5$, $m = 4$.

Fig. 8. Channel threshold γ versus the average number of successfully decoded bits $\bar{\mathcal{C}}_{\text{suc}}$ for different user pairing schemes.

F. Impact of User Pairing

In this work, we have considered a simple user pairing scheme, i.e., random selection, and demonstrated the advantage of properly setting the reflection coefficients. In this subsection, as inspired from [32], we consider two user pairing schemes with selection rules and show that properly setting the reflection coefficients is still beneficial. The following two user pairing schemes with selection rules are considered:

- Scheme 1: k-th strongest signal is paired with k-th weakest signal (equivalently, $M + 1 - k$-th strongest signal), where $k \in [1, M/2]$.
- Scheme 2: k-th strongest signal is paired with the $M+k$-th strongest signal, where $k \in [1, M/2]$.

Fig. 8 plots the average number of successfully decoded bits versus the channel threshold for different user pairing schemes. The results for Schemes 1 and 2 are generated using Matlab simulation. From Fig. 8, we can see that, when the channel threshold is small, Scheme 2 performs the best. However,

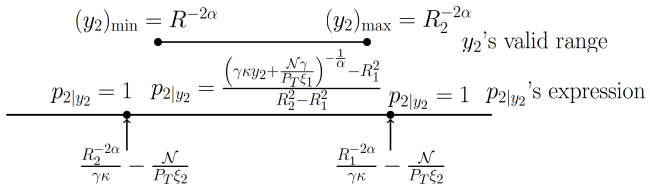

Fig. 9. Illustration of expressions of $p_{2|y_2}$ and the valid range of y_2 when $\frac{R_1^{-2\alpha}}{\gamma\kappa} - \frac{R_2^{-2\alpha}}{\gamma\kappa} \geq R_2^{-2\alpha} - R^{-2\alpha}$.

while the channel threshold is large, our considered scheme can perform the best. The key insight from Fig. 8 is that setting the reflection coefficients for the paired BNs differently benefits all the schemes. The reflection coefficient selection criteria for the general multiplexing scenario needs careful investigation for different user pairing schemes and is left for future work.

VII. Conclusions

In this work, we have come up with a BackCom system enhanced by the power-domain NOMA, i.e., multiplexing the BNs located in different spatial regions or with different reflected power levels. Especially, the reflection coefficients for the BNs coming from different groups are set to be different such that the NOMA is fully utilized (i.e., increase the channel gain different for multiplexing BNs). In order to optimize the system performance, we provided the criteria for choosing the reflection coefficients for different groups of BNs. We also derived the analytical results for the average number of successfully decoded bits for two-node pairing case and the average number of successful BNs for the general multiplexing case. These derived results validated our proposed selection criteria. Our numerical results illustrated that NOMA generally results in the much better performance gain in the BackCom system than its performance gain in the conventional system. This demonstrated the significance of adopting NOMA with the BackCom system. Future work can consider the multiple readers scenario and the BNs powered by power beacons or ambient RF signals.

Appendix A

Proof: Since we consider the $\xi_1 \geq \xi_2$ scenario, the decoding order is always from the near BN to the far BN. The probability that both BNs are successfully decoded is given by

$$\begin{aligned} p_2 &= \Pr\left(\frac{P_T\xi_1 r_1^{-2\alpha}}{P_T\xi_2 r_2^{-2\alpha} + \mathcal{N}} \geq \gamma \;\&\&\; \frac{P_T\xi_2 r_2^{-2\alpha}}{\mathcal{N}} \geq \gamma\right) \\ &= \Pr\left(y_1 \geq \gamma\kappa y_2 + \frac{\mathcal{N}\gamma}{P_T\xi_1} \;\&\&\; y_2 \geq \frac{\mathcal{N}\gamma}{P_T\xi_2}\right) \\ &= \begin{cases} 0, & \frac{\mathcal{N}\gamma}{P_T\xi_2} \geq R_2^{-2\alpha}; \\ \int_{\min\left\{\frac{\mathcal{N}\gamma}{P_T\xi_2}, R^{-2\alpha}\right\}}^{R_2^{-2\alpha}} p_{2|y_2} f_{y_2}(y_2)\mathrm{d}y_2, & \frac{\mathcal{N}\gamma}{P_T\xi_2} < R_2^{-2\alpha}; \end{cases} \end{aligned} \tag{28}$$

where $y_1 \triangleq r_1^{-2\alpha}$ with PDF $f_{y_1}(y_1) = \frac{y_1^{-\frac{1}{\alpha}-1}}{\alpha(R_2^2 - R_1^2)}$ and $y_1 \in \left[R_2^{-2\alpha}, R_1^{-2\alpha}\right]$, $y_2 \triangleq r_2^{-2\alpha}$ with PDF $f_{y_2}(y_2) = \frac{y_2^{-\frac{1}{\alpha}-1}}{\alpha(R^2 - R_2^2)}$ and $y_2 \in \left[R^{-2\alpha}, R_2^{-2\alpha}\right]$, and $p_{2|y_2}$ is the conditional probability of p_2.

We first consider the case of $\frac{\mathcal{N}\gamma}{P_T\xi_2} < R^{-2\alpha}$, which implies that the weaker signal can be always successfully decoded given that the stronger signal is successfully decoded. Note that when $\gamma\kappa y_2 + \frac{\mathcal{N}\gamma}{P_T\xi_1} \leq (y_1)_{\min} = R_2^{-2\alpha}$ (e.g., $y_2 \leq \frac{R_2^{-2\alpha}}{\gamma\kappa} - \frac{\mathcal{N}}{P_T\xi_2}$), the conditional probability $p_{2|y_2}$ is always equal to one. When $\gamma\kappa y_2 + \frac{\mathcal{N}\gamma}{P_T\xi_1} \geq (y_1)_{\max} = R_1^{-2\alpha}$ (e.g., $y_2 \geq \frac{R_1^{-2\alpha}}{\gamma\kappa} - \frac{\mathcal{N}}{P_T\xi_2}$), $p_{2|y_2}$ is always equal to zero. For the remaining range of y_2, $p_{2|y_2} = \int_{\gamma\kappa y_2 + \frac{\mathcal{N}\gamma}{P_T\xi_1}}^{R_1^{-2\alpha}} \frac{y_1^{-\frac{1}{\alpha}-1}}{\alpha(R_2^2 - R_1^2)}\mathrm{d}y_1 = \frac{\left(\gamma\kappa y_2 + \frac{\mathcal{N}\gamma}{P_T\xi_1}\right)^{-\frac{1}{\alpha}} - R_1^2}{R_2^2 - R_1^2}$.

Based on the expressions of $p_{2|y_2}$ and y_2's valid range, when $\frac{R_1^{-2\alpha}}{\gamma\kappa} - \frac{R_2^{-2\alpha}}{\gamma\kappa} \geq R_2^{-2\alpha} - R^{-2\alpha}$, we can plot a diagram in Fig. 9 to help finding the integration limits. From Fig. 9, we obtain the final expression of p_2 as

- $\gamma \leq \frac{R_2^{-2\alpha}}{\kappa R_2^{-2\alpha} + \frac{\mathcal{N}}{P_T\xi_1}}$: $p_2 = 1$;
- $\gamma \geq \frac{R_1^{-2\alpha}}{\kappa R^{-2\alpha} + \frac{\mathcal{N}}{P_T\xi_1}}$: $p_2 = 0$;
- Other range:

$$\begin{aligned} p_2 = &\int_{R^{-2\alpha}}^{\max\left\{\frac{R_2^{-2\alpha}}{\gamma\kappa} - \frac{\mathcal{N}}{P_T\xi_2}, R^{-2\alpha}\right\}} f_{y_2}(y_2)\mathrm{d}y_2 \;+ \\ &\int_{\max\left\{\frac{R_2^{-2\alpha}}{\gamma\kappa} - \frac{\mathcal{N}}{P_T\xi_2}, R^{-2\alpha}\right\}}^{\min\left\{\frac{R_1^{-2\alpha}}{\gamma\kappa} - \frac{\mathcal{N}}{P_T\xi_2}, R_2^{-2\alpha}\right\}} \frac{\left(\gamma\kappa y_2 + \frac{\mathcal{N}\gamma}{P_T\xi_1}\right)^{-\frac{1}{\alpha}} - R_1^2}{R_2^2 - R_1^2} f_{y_2}(y_2)\mathrm{d}y_2. \end{aligned}$$

We note the above expressions of p_2 also hold for $\frac{R_1^{-2\alpha}}{\gamma\kappa} - \frac{R_2^{-2\alpha}}{\gamma\kappa} < R_2^{-2\alpha} - R^{-2\alpha}$. For other cases, we can adopt the similar steps to work out p_2. After further computation and simplification, we arrive at the result in (4). ■

References

[1] M. Shirvanimoghaddam, M. Dohler, and S. J. Johnson, "Massive non-orthogonal multiple access for cellular IoT: Potentials and limitations," *IEEE Commun. Mag.*, vol. 55, no. 9, pp. 55–61, Sep. 2017.

[2] Z. Dawy, W. Saad, A. Ghosh, J. G. Andrews, and E. Yaacoub, "Towards massive machine type cellular communications," *IEEE Wireless Commun.*, vol. 24, no. 1, pp. 120–128, Feb. 2017.

[3] Y. Mehmood, N. Haider, M. Imran, A. Timm-Giel, and M. Guizani, "M2M communications in 5G: State-of-the-art architecture, recent advances, and research challenges," *IEEE Commun. Mag.*, vol. 55, no. 9, pp. 194–201, Sep. 2017.

[4] D. N. K. Jayakody, J. Thompson, S. Chatzinotas, and S. Durrani, *Wireless Information and Power Transfer: A New Paradigm for Green Communications*. Springer International Publishing AG, 2017.

[5] W. Liu, K. Huang, X. Zhou, and S. Durrani, "Next generation backscatter communication: Theory and applications," 2017, submitted. [Online]. Available: https://arxiv.org/abs/1701.07588

[6] C. Boyer and S. Roy, "Backscatter communication and RFID: Coding, energy, and MIMO analysis," *IEEE Trans. Commun.*, vol. 62, no. 3, pp. 770–785, Mar. 2014.

[7] G. Vannucci, A. Bletsas, and D. Leigh, "A software-defined radio system for backscatter sensor networks," *IEEE Trans. Wireless Commun.*, vol. 7, no. 6, pp. 2170–2179, Jun. 2008.

[8] A. Bletsas, S. Siachalou, and J. N. Sahalos, "Anti-collision backscatter sensor networks," *IEEE Trans. Wireless Commun.*, vol. 8, no. 10, pp. 5018–5029, Oct. 2009.

[9] J. Kimionis, A. Bletsas, and J. N. Sahalos, "Increased range bistatic scatter radio," *IEEE Trans. Commun.*, vol. 62, no. 3, pp. 1091–1104, Mar. 2014.

[10] W. Saad, X. Zhou, Z. Han, and H. V. Poor, "On the physical layer security of backscatter wireless systems," *IEEE Trans. Wireless Commun.*, vol. 13, no. 6, pp. 3442–3451, Jun. 2014.

[11] W. Liu, K. Huang, X. Zhou, and S. Durrani, "Full-duplex backscatter interference networks based on time-hopping spread spectrum," *IEEE Trans. Wireless Commun.*, vol. 16, no. 7, pp. 4361–4377, Jul. 2017.

[12] V. Liu, A. Parks, V. Talla, S. Gollakota, D. Wetherall, and J. R. Smith, "Ambient backscatter: Wireless communication out of thin air," in *Proc. SIGCOMM*, 2013, pp. 39–50.

[13] G. Yang, Y.-C. Liang, R. Zhang, and Y. Pei, "Modulation in the air: Backscatter communication over ambient OFDM carrier," 2017, submitted. [Online]. Available: https://arxiv.org/abs/1704.02245

[14] K. Han and K. Huang, "Wirelessly powered backscatter communication networks: Modeling, coverage, and capacity," *IEEE Trans. Wireless Commun.*, vol. 16, no. 4, pp. 2548–2561, Apr. 2017.

[15] M. Bacha and B. Clerckx, "Backscatter communications for the internet of things: A stochastic geometry approach," 2017, submitted. [Online]. Available: https://arxiv.org/abs/1711.07277

[16] G. Yang, C. K. Ho, and Y. L. Guan, "Multi-antenna wireless energy transfer for backscatter communication systems," *IEEE J. Sel. Areas Commun.*, vol. 33, no. 12, pp. 2974–2987, Dec. 2015.

[17] C. Psomas and I. Krikidis, "Backscatter communications for wireless powered sensor networks with collision resolution," *IEEE Wireless Commun. Lett.*, vol. 6, no. 5, pp. 650–653, Oct. 2017.

[18] G. Zhu, S.-W. Ko, and K. Huang, "Inference from randomized transmissions by many backscatter sensors," *IEEE Trans. Wireless Commun.*, vol. 17, no. 5, pp. 3111–3127, May 2018.

[19] Z. Ding, X. Lei, G. K. Karagiannidis, R. Schober, J. Yuan, and V. Bhargava, "A survey on non-orthogonal multiple access for 5G networks: Research challenges and future trends," *IEEE J. Sel. Areas Commun.*, vol. 35, no. 10, pp. 2181–2195, Oct. 2017.

[20] W. Shin, M. Vaezi, B. Lee, D. J. Love, J. Lee, and H. V. Poor, "Non-orthogonal multiple access in multi-cell networks: Theory, performance, and practical challenges," *IEEE Commun. Mag.*, vol. 55, no. 10, pp. 176–183, Oct. 2017.

[21] M. Al-Imari, P. Xiao, M. A. Imran, and R. Tafazolli, "Uplink nonorthogonal multiple access for 5G wireless networks," in *Proc. ISWCS*, 2014, pp. 781–785.

[22] Z. Yang, Z. Ding, P. Fan, and N. Al-Dhahir, "A general power allocation scheme to guarantee quality of service in downlink and uplink NOMA systems," *IEEE Trans. Wireless Commun.*, vol. 15, no. 11, pp. 7244–7257, Nov. 2016.

[23] M. A. Sedaghat and R. R. Muller, "On user pairing in NOMA uplink," *IEEE Trans. Wireless Commun.*, vol. 17, no. 5, pp. 3474–3486, May 2018.

[24] P. D. Diamantoulakis, K. N. Pappi, Z. Ding, and G. K. Karagiannidis, "Wireless-powered communications with non-orthogonal multiple access," *IEEE Trans. Wireless Commun.*, vol. 15, no. 12, pp. 8422–8436, Dec. 2016.

[25] P. Deng, B. Wang, W. Wu, and T. Guo, "Transmitter design in MISO-NOMA system with wireless-power supply," *IEEE Commun. Lett.*, vol. 22, no. 4, pp. 844–847, Apr. 2018.

[26] Q. Wu, W. Chen, D. W. K. Ng, and R. Schober, "Spectral and energy efficient wireless powered IoT networks: NOMA or TDMA?" *IEEE Trans. Veh. Technol.*, vol. 67, no. 7, pp. 6663–6667, Jul. 2018.

[27] B. Lyu, Z. Yang, G. Gui, and H. Sari, "Optimal time allocation in backscatter assisted wireless powered communication networks," *Sensors*, vol. 17, no. 6, 2017.

[28] Z. Khalid and S. Durrani, "Distance distributions in regular polygons," *IEEE Trans. Veh. Technol.*, vol. 62, no. 5, pp. 2363–2368, Jun. 2013.

[29] M. Wildemeersch, T. Q. S. Quek, M. Kountouris, A. Rabbachin, and C. H. Slump, "Successive interference cancellation in heterogeneous networks," *IEEE Trans. Commun.*, vol. 62, no. 12, pp. 4440–4453, Dec. 2014.

[30] M. Raab and A. Steger, "Balls into bins-A simple and tight analysis," in *Lecture Notes in Computer Science*, 1998, pp. 159–170.

[31] J. Guo, S. Durrani, and X. Zhou, "Outage probability in arbitrarily-shaped finite wireless networks," *IEEE Trans. Commun.*, vol. 62, no. 2, pp. 699–712, Feb. 2014.

[32] Z. Ding, P. Fan, and H. V. Poor, "Impact of user pairing on 5G nonorthogonal multiple-access downlink transmissions," *IEEE Trans. Veh. Technol.*, vol. 65, no. 8, pp. 6010–6023, Aug. 2016.

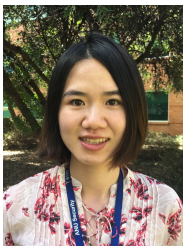

Jing Guo (S'12-M'17) received her BSc (first class honours) in electronics and telecommunications engineering from the Australian National University, Australia and the Beijing Institute of Technology, China in 2012, and PhD degree in telecommunications engineering from the Australian National University in 2016. She is currently employed as a Postdoctoral Research Fellow at the Research School of Engineering, Australian National University, Canberra, Australia. Her research interest lies in the field of wireless communications, including machine-to-machine communications and the application of stochastic geometry to wireless networks.

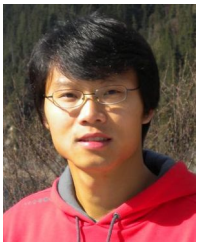

Xiangyun Zhou (SM'17-M'11) is a Senior Lecturer at the Australian National University (ANU). He received the Ph.D. degree in telecommunications engineering from ANU in 2010. His research interests are in the fields of communication theory and wireless networks. He currently serves on the editorial board of IEEE TRANSACTIONS ON WIRELESS COMMUNICATIONS and IEEE COMMUNICATIONS LETTERS. He served as a guest editor for IEEE COMMUNICATIONS MAGAZINE's feature topic on wireless physical layer security in 2015. He also served as symposium/track and workshop co-chairs for major IEEE conferences. He was the chair of the ACT Chapter of the IEEE Communications Society and Signal Processing Society from 2013 to 2014. He is a recipient of the Best Paper Award at ICC'11 and IEEE ComSoc Asia-Pacific Outstanding Paper Award in 2016.

Salman Durrani (S'00-M'05-SM'10) received the B.Sc. (1st class honours) degree in Electrical Engineering from the University of Engineering & Technology, Lahore, Pakistan in 2000. He received the PhD degree in Electrical Engineering from the University of Queensland, Brisbane, Australia in Dec. 2004. He has been with the Australian National University, Canberra, Australia, since 2005, where he is currently Associate Professor in the Research School of Engineering, College of Engineering & Computer Science.

His research interests are in wireless communications and signal processing, including machine-to-machine and device-to-device communication, wireless energy harvesting systems, stochastic geometry modelling of finite area networks and synchronization in communication systems. He has co-authored more than 130 publications to date in refereed international journals and conferences. He was a recipient of the 2016 IEEE ComSoc Asia Pacific Outstanding Paper Award. He was the Chair of the ACT Chapter of the IEEE Signal Processing and Communications Societies from 2015 to 2016. He currently serves as an Editor of the IEEE TRANSACTIONS ON COMMUNICATIONS. He was awarded the 2018 ANU VC Award for Excellence in Supervision and the 2012 ANU VC Award for Excellence in Education. He is a Member of Engineers Australia, a Senior Fellow of IEEE, USA and a Senior Fellow of The Higher Education Academy, UK.

Halim Yanikomeroglu (F'17) was born in Giresun, Turkey, in 1968. He received the B.Sc. degree in electrical and electronics engineering from the Middle East Technical University, Ankara, Turkey, in 1990, and the M.A.Sc. degree in electrical engineering (now ECE) and the Ph.D. degree in electrical and computer engineering from the University of Toronto, Canada, in 1992 and 1998, respectively.

During 1993-1994, he was with the R&D Group of Marconi Kominikasyon A.S., Ankara, Turkey. Since 1998 he has been with the Department of Systems and Computer Engineering at Carleton University, Ottawa, Canada, where he is now a Full Professor. His research interests cover many aspects of wireless technologies with a special emphasis on cellular networks. Dr. Yanikomeroglu has supervised 18 PhD and 28 MASc theses (all completed); several of his PhD students received various medals. He has coauthored 350+ peer-reviewed research papers including about 120 in the IEEE journals. He has been one of the most frequent tutorial presenters in the leading international IEEE conferences (29 times). He has had extensive collaboration with large-scale (such as Huawei, Samsung, Blackberry, Telus, Nortel), medium-scale, and small-scale companies as well as the government labs (such as Communications Research Centre of Canada). During 2012-2016, he led one of the largest academic-industrial collaborative research project on pre-standards 5G wireless networks. Dr. Yanikomeroglu's collaborative research resulted in 24 granted patents (plus about 15 applied).

Dr. Yanikomeroglu is a Fellow of the IEEE with the citation "for contributions to wireless access architectures in cellular networks". He is a Distinguished Lecturer for the IEEE Communications Society and a Distinguished Speaker for the IEEE Vehicular Technology Society. He has been involved in the organization of the IEEE Wireless Communications and Networking Conference (WCNC) from its inception in 1998 in various capacities including serving as a Steering Committee member for a decade and the Technical Program Chair/Co-Chair of WCNC 2004 (Atlanta), WCNC 2008 (Las Vegas), and WCNC 2014 (Istanbul). He was the General Co-Chair of the IEEE 72nd Vehicular Technology Conference (VTC 2010-Fall) held in Ottawa, and the General Chair of the IEEE 86th Vehicular Technology Conference (VTC 2017-Fall) held in Toronto. He has served in the editorial boards of the IEEE Transactions on Communications, IEEE Transactions on Wireless Communications, and IEEE Communications Surveys & Tutorials; he also served as a guest editor in various IEEE journal special issues. He was the Chair of one of the largest technical committees in IEEE, Technical Committee on Personal Communications (now called Wireless Communications Technical Committee and has 1,700+ members).

Dr. Yanikomeroglu is a recipient of the IEEE Ottawa Section Outstanding Educator Award in 2014, Carleton University Faculty Graduate Mentoring Award in 2010, the Carleton University Graduate Students Association Excellence Award in Graduate Teaching in 2010, and the Carleton University Research Achievement Award in 2009 and 2018. Dr. Yanikomeroglu spent the 2011-2012 academic year at TOBB U. of Economics and Technology, Ankara, Turkey, as a Visiting Professor. He is a registered Professional Engineer in the province of Ontario, Canada.